High Speed Control of Atom Transfer Sequence from Magneto-Optical to Dipole Trap for Quantum Computing

A Senior Project

Presented To

The Faculty of the Physics Department

California Polytechnic State University, San Luis Obispo

In Partial Fulfillment

of the Requirements for the Degree

Bachelor of Arts

by

Jason Garvey Schray

December, 2014

Table of Contents

List of Figures

List of Tables

Abstract

Two circuits were designed, built, and tested for the purpose of aiding in the transfer of ^{87}Rb atoms from a MOT to dipole traps and for characterizing the final dipole traps. The first circuit was a current switch designed to quickly turn the magnetic fields of the MOT off. The magnetic coil switch was able to reduce the magnetic field intensity to 5 % of its initial value after 81 μs. The second circuit was an analog signal switch designed to turn the modulation signal of an AOM off. The analog switch was able to reduce the modulation signal intensity to 8.5 % of its initial magnitude in ~25μs. The performances of the two circuits discussed in this paper are sufficient for future atom transfer research based on predicted experimental requirements.

1: Introduction

Computing technology has changed every facet of modern day life. From social networking and personal finances to communications and even academic research, computers have realized concepts that were previously thought to be impossible. For all of the wonderful things that computers can accomplish, there are only two different functions that a system must fulfill to be considered a modern computing device: the computer must have some form of memory and the computer must be able to perform computations on that memory. The forms that these two requirements can take vary from system to system, but usually fall into two categories: analog and digital systems.

1.1 Types of computers

Analog computers deal with continuous values and typically are constantly doing calculations on continuous data sets. One example of these computers is an analog controls system. An analog controls system constantly reads an incoming value, and combines that with data in its analog memory to determine an appropriate output to control something. Another example of these systems exists where analog computing is used in high-speed processors. It turns out that analog computers are actually well suited to some problems that digital computers are quite slow at such as exponential operators (e.g. taking the square root of a number).

People are more familiar with digital computers. These computers deal with binary values (0 or 1) and do computations at discrete time intervals. Examples of these kinds of systems are personal computers and modern cell phones. Figure 1-1 shows examples of the analog and digital waveforms.

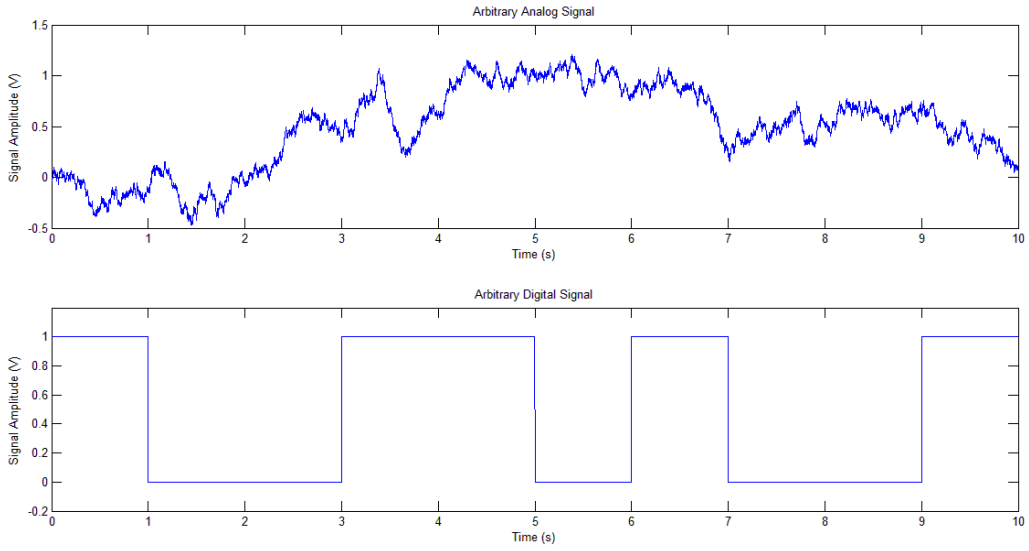

Figure 1-1 - The top plot represents an analog signal. The bottom plot represents a digital signal.

While classical computers come in many different flavors, there are limits to their ability to solve certain problems. Classical computers are quite efficient at sorting and performing basic arithmetic operations. That being said, there are still a few problems that modern computing technology can't solve in a reasonable time frame: factoring prime numbers, data searching, simulating many bodied quantum systems, etc. Quantum computers promise to solve some of these problems.

Up until now, all of the computing devices discussed have been classical computers. Quantum computers are a variant on these systems that aim to utilize quantum mechanical effects to improve the efficiency of solving certain problems. Like classical computers, quantum computers can come in both

analog forms and digital forms. This paper will be discussing primarily digital models of a quantum computer.

The main quantum phenomenon that promises to improve upon classical computing performance is the phenomenon of superposition. For a digital classical computer, memory is typically made of single bits (some logic systems exist that incorporate tertiary or m-level units of memory but they are not common). These bits can take on the binary values of either 1 or 0. If a classical computer performs an operation on a classical bit, the result of the computation will be either 1 or 0. Quantum systems do not operate in quite the same way. Quantum bits (also known as qubits) can actually be in a superposition of states where they have a probability of being both 0 and 1 at the same time. When a quantum operation is performed, the resultant value of the qubit can actually still be in a superposition of 1 and 0. In fact with n bits, 2^n possible numbers can be processed at the same time. Unfortunately, the resulting quantum outputs have to be measured many times to map out the quantum state but for some algorithms that don't need to measure the resulting quantum states, a significant increase in processing speed can be achieved (e.g. Shor's Algorithm[1]).

Another trait of quantum systems that is important for quantum algorithms is entanglement. Entanglement is the ability for a measurement of one qubit to affect the state of another qubit. If two qubits are entangled and both are in a superposition of states, once the first qubit is measured, the state of the second qubit will be altered. This phenomenon forms the basis for two-qubit gates.

1.2 Quantum Computer Requirements

DiVincenzo[2] has listed a set of requirements that quantum computing schemes are encouraged to meet in order to form a successful quantum computer. While these requirements aren't everything, they do provide a minimum set of goals by which any experimental approach to quantum computing should measure its success and discern problems to address. These requirements are: the qubits must be well characterized and scalable, the qubits must be able to be initialized into a known state, they must have relatively long decoherence times, the qubits must be readable so that their state distribution can be known, and the qubits must be able to go through a universal set of gates.

A universal set of quantum gates is made of any set of gates that are sufficient for any possible quantum algorithm. For example, a Haddamard gate, π/8 gate, and a controlled not gate make up a universal set of quantum gates. Below is a brief description of a few examples of suggested quantum computer archetypes being pursued and what their strengths and weaknesses are when considering DiVincenzo's list.

2.2.1 Nuclear Magnetic Resonance Qubits

Nuclear magnetic resonance (NMR) quantum computing uses the spin states of electrons in a molecule as qubits. The qubits are relatively easy to build and were used in the first successful implementation of Shor's algorithm[3] to factor the number 15. However, NMR qubits fail DiVincenzo's first requirement of scalability because scaling this technique to large numbers of qubits requires extremely large molecules.

2.2.2 Optical Qubits

Optical qubits can be the presence of photons in an optical cavity, the polarization of photons, the frequency of photons, or the time of arrival of photons at a detector[4]. Optical qubits are attractive for communications applications, because photons travel at the speed of light and can thus quickly carry quantum information over large distances.

2.2.3 Ion Qubits

Ions can be trapped with a high degree of control using electromagnetic fields. The qubit is typically represented by energy levels of the ions. There have been many proposed topologies for scaling ion qubits to large numbers. To date, the largest number of ions to be entangled at once has been 14 ions[5]. The main issue that this technique has encountered is strong coupling to its environment and short decoherence times.

2.2.4 Neutral Atom Qubits

Neutral atoms can be trapped in both magnetic and optical traps. Their qubits are usually represented by hyperfine atomic energy levels. It is difficult to scale up to large numbers of neutral atoms in an addressable array. Otherwise, neutral atom qubits fulfill all of the requirements put forth by DiVincenzo.

1.3 Optical Dipole Trap Overview

Neutral atoms can be trapped using a variety of different methods. One such method of traps has been optical traps. In an optical dipole trap, the laser's frequency is set to be slightly off-resonance with an atomic transition (laser detuning). If the laser's frequency is slightly greater than the atomic transition, the laser is said to be blue detuned and if it is slightly less than the transition it is said to be red detuned. Blue detuned laser light repels atoms and red detuned light attracts them. The strength of repulsion or attraction is dependent on both the detuning and the intensity of the laser. In this way laser light patterns can serve as localized dipole traps. In the most optimal space efficiency, three dimensional (2-D) lattices of optical traps have been assembled and used to successfully trap neutral atoms. Unfortunately a perfect 3-D lattice isn't optimal for scalable quantum computing due to the difficulty with which individual atoms are addressed inside the lattice. A solution to this problem would be a two dimensional (2-D) lattice. Several approaches to creating a 2-D lattice have been explored: counter propagating laser beams[6], 2-D arrays of microlenses[7], and evanescent waves above waveguides.

Our present approach is to use the diffraction pattern behind a pinhole to generate a localized bright or dark spot for a detuned dipole trap[8]. If this trap can be implemented successfully then it could be scaled up to multiple traps in a 2-D lattice behind a 2-D array of pinholes. Figure 1-2 displays a diagram of a calculated diffraction behind a pinhole.

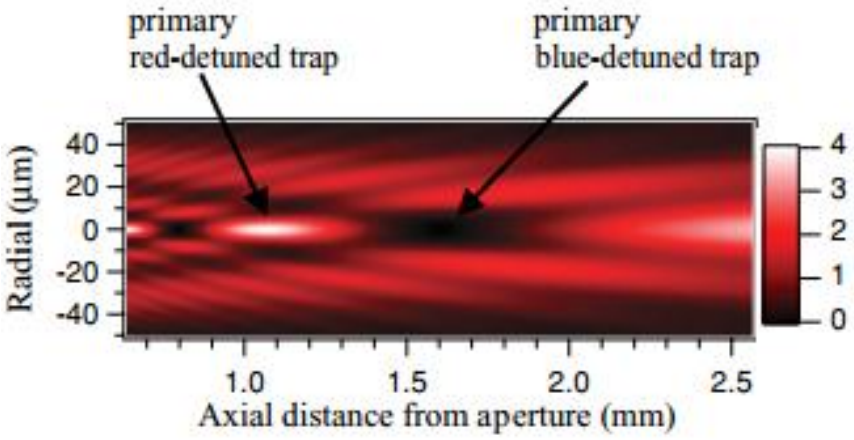

Figure 1-2 - Calculated pinhole dipole trap intensity profile[9].

2: Theory

The final goal of this research group is to test pinhole dipole traps. The first step in testing any atom trap is to first cool it using a magneto optical trap (MOT). Atoms trapped n MOTs typically have kinetic energies corresponding to 200 μK or less expressed in terms of temperature. If the potential energy of the pinhole dipole traps exceeds this energy then the atoms can be trapped in the pinhole dipole traps. Atoms trapped in the appropriate dipole traps can then be used for quantum computations. This chapter covers how a MOT works, how to transfer atoms from a MOT to dipole traps, and how to characterize those dipole traps.

2.1 General Background of the Experimental Setup

For this project, there are two different systems that have been tested independently. The MOT, which initially collects and cools a large number of ^{87}Rb atoms, and the dipole trap, where those cooled atoms will be transferred. The following sections give a brief overview of how a MOT works and how this project plans to implement dipole traps.

3.1.1 MOT Overview

The main purpose of a MOT is to cool and collect large numbers of atoms. MOTs operate on three different principles: Doppler cooling, Zeeman splitting, and atomic transition selection rules.

3.1.1.A Doppler Cooling

Doppler cooling works on the principle that a moving atom will see a Doppler shift in a laser's wavelength based on its motion relative to that laser. To understand this, first consider what occurs during the absorption of laser light by ^{87}Rb atoms as shown in Figure 2-1.

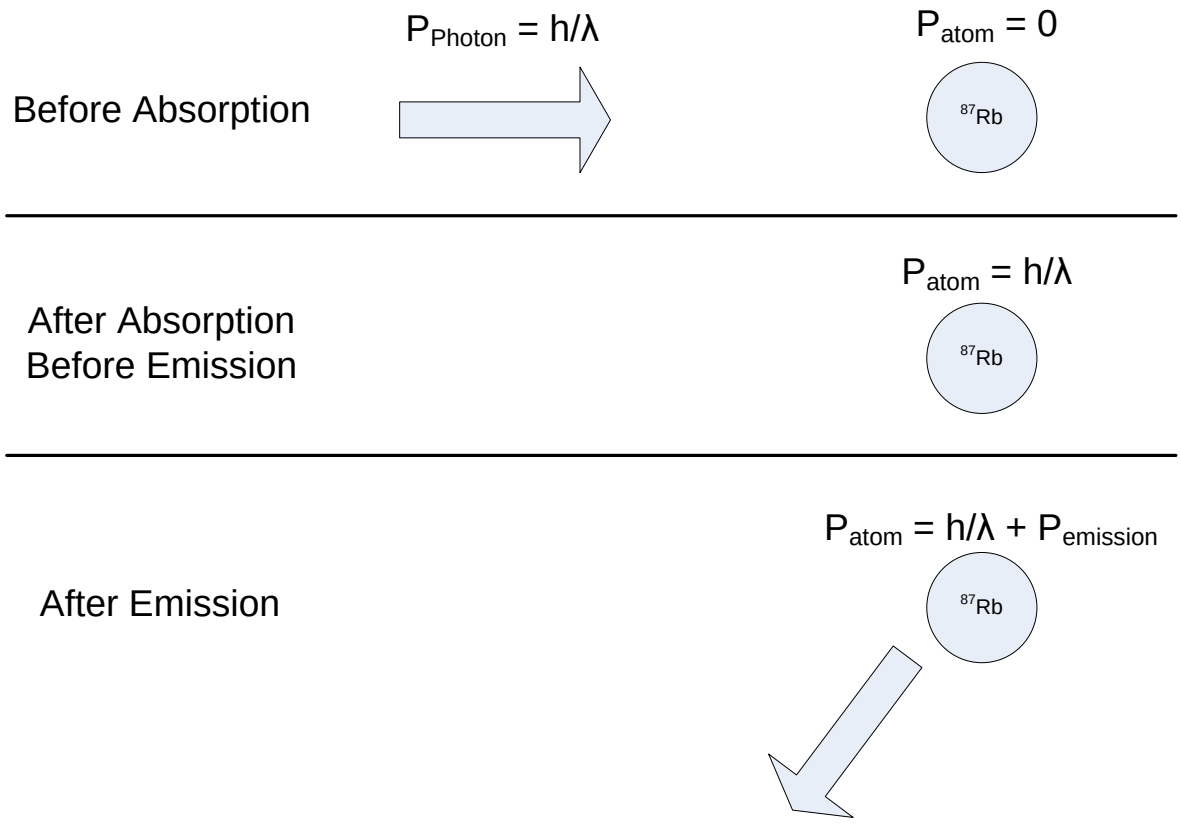

Figure 2-1 - Absorption and emission of laser light by ^{87}RB.

The atom's total momentum shift during this process is given by (2-1).

$$\overrightarrow{\Delta p} = \overrightarrow{P_{photon}} + \overrightarrow{P_{emission}} \quad (2\text{-}1)$$

In (2-1), $\overrightarrow{\Delta p}$ represents the momentum shift of the atom, $\overrightarrow{P_{photon}}$ represents the component of $\overrightarrow{\Delta p}$ from the absorption of the laser photon, and $\overrightarrow{P_{emission}}$ represents the component of $\overrightarrow{\Delta p}$ due to the spontaneous emission of that photon. The direction of $\overrightarrow{\Delta p}$ is unknown for a single photon absorption/emission interaction. It is known, however, that the direction of $\overrightarrow{P_{emission}}$ for spontaneous emission is uniformly random and so if a large number N of photons is absorbed over a long period of time, the total momentum kick can be shown to be given by (2-2).

$$\overrightarrow{\Delta P_{total}} = \sum_{i=1}^{N} \overrightarrow{\Delta p_i} \approx N\overrightarrow{P_{photon}} \quad (2\text{-}2)$$

In equation (2-2), $\overrightarrow{\Delta P_{total}}$ represents the total momentum gained by the atom over many absorption/emission interactions. In this way, a laser can exert a force on an atom by imparting momentum to it.

The interaction shown in Figure 2-1 only can occur if the frequency of the laser is tuned to an allowable transition of ^{87}RB. If the frequency of the laser is slightly off resonance with respect to the atom, then the atom will rarely absorb the photon and will feel little force from the laser. To cool atoms, a MOT laser must exert a force on atoms that are moving. Lasers can be tuned to only exert forces on moving atoms, because light experiences a reference frame dependent Doppler shift given by (2-3).

$$\lambda_o = \lambda_s \sqrt{\frac{c-v}{c+v}} \quad (2\text{-}3)$$

In (2-3) λ_o is the wavelength of the laser seen by the observer, λ_s is the wavelength of the laser seen by the source, v is the velocity of the observer away from the source , and c is the speed of light. Figure 2-2 shows the possible interactions between detuned lasers and moving ^{87}Rb atoms.

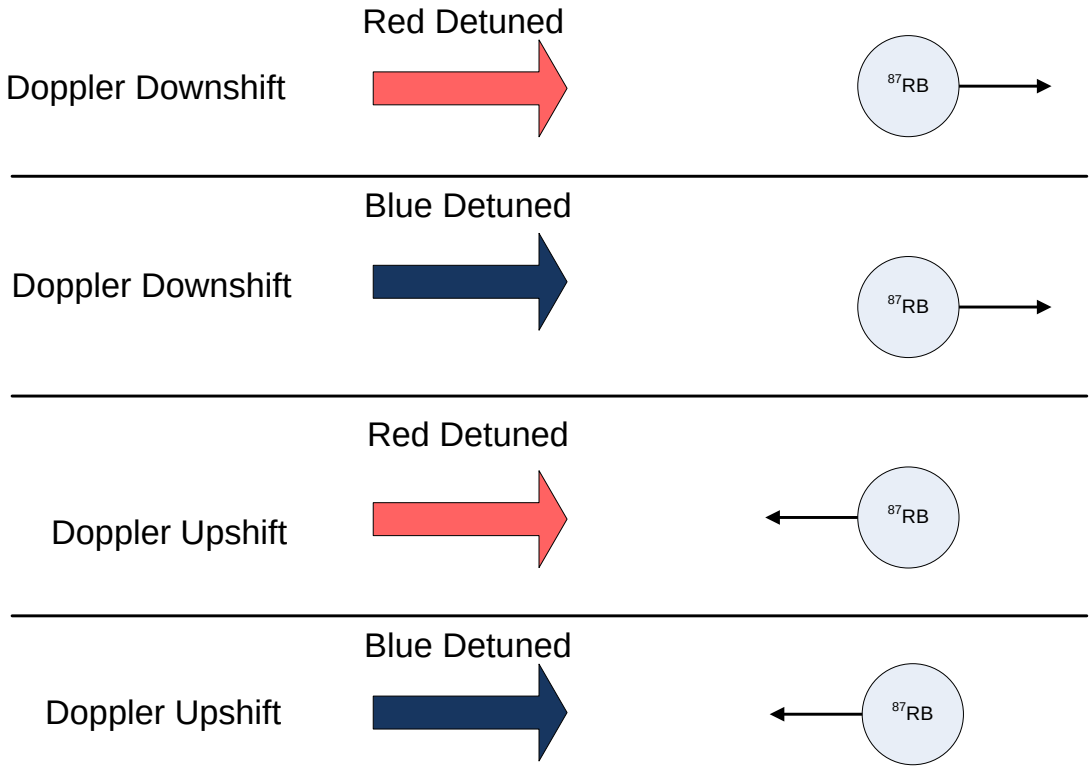

Figure 2-2 - Detuned laser interactions with moving ^{87}Rb atoms.

In Figure 2-2, the only interaction where the laser exerts a force opposite to the motion of the ^{87}Rb is the third interaction between a red-shifted laser and rubidium traveling in the opposite direction as the laser. When this occurs, the atom will absorb the laser photons and feel a force that slows its motion. In the first interaction shown, the same red-shifted laser doesn't interact with the ^{87}Rb because the Doppler shift is in the wrong direction and the laser is farther detuned from the absorption frequency. Therefore, sending in red detuned laser beams from all directions of space will slow down (cool) the atoms regardless of which way they were moving.

3.1.1.B Selection Rules

The next important mechanism that is required in a MOT is the ability to maintain atoms in the appropriate state to absorb photons. Figure 2-3 shows the hyperfine structure of ^{87}RB and the different possible state transitions that occur in a MOT.

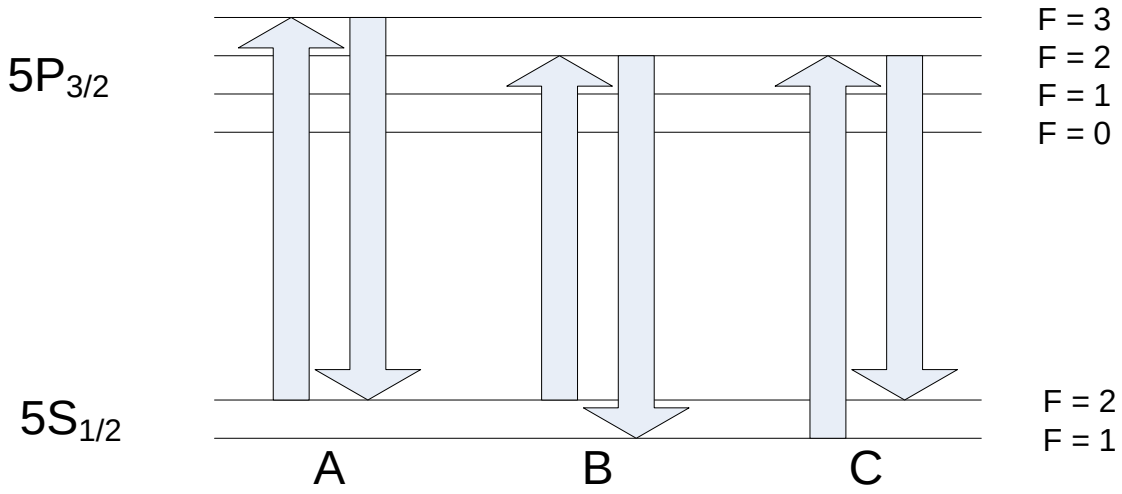

Figure 2-3 - ^{87}RB hyperfine structure. A: normal MOT atom "cycling" transition. B: decay into "dark" hyperfine state. C: repump into MOT cooling states.

The transition designated by A shows the normal absorption and emission of a MOT laser, the so-called "cycling" transition. The transition designated by B shows a possibility that the MOT lasers can excite the atom into the F=2 state from which it can decay into the F=1 ground state. In the F=1 ground state, the atom cannot absorb the same photons as in the A transition. To insure that all atoms in the MOT are in the F=2 ground state a second laser pumps the atoms in the F=1 ground state into the F=2 excited state where they can decay back into the F=2 ground state. This transition is designated by C in Figure 2-3. With these three mechanisms, a MOT collects atoms and cools them to approximately 200 μK. Thus, operating a MOT requires two frequencies: F=2 → F=3 (trap laser) and F=1 → F=2 (repump laser).

3.1.1.C Zeeman Effect

The Doppler cooling effect does cool the atoms, but without some other force, the atoms would never collect into a known location within the MOT. To collect the atoms in the center, the MOT sets up a magnetic field within the MOT vacuum chamber. The magnetic field at the center of the chamber is non-existent and increases in value with any displacement from the chamber's center as shown in Figure 2-4.

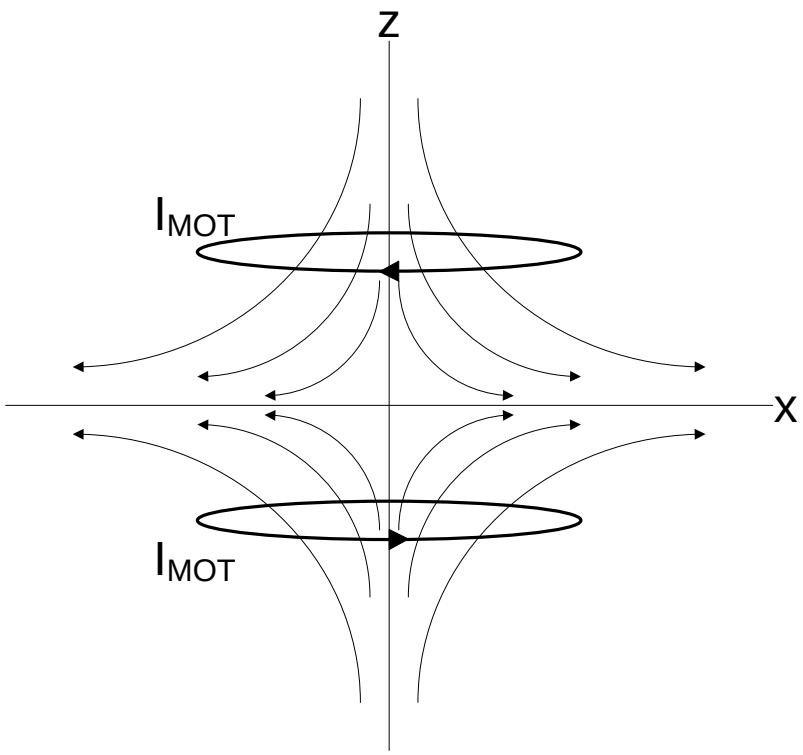

Figure 2-4 - MOT magnetic field from antiparallel Helmholtz coils.

Due to the Zeeman effect, the F=2→F=3 transition energy becomes proportional to the magnetic field intensity near the origin. Figure 2-5 shows a simplified energy diagram of the F=2→F=3 transition.

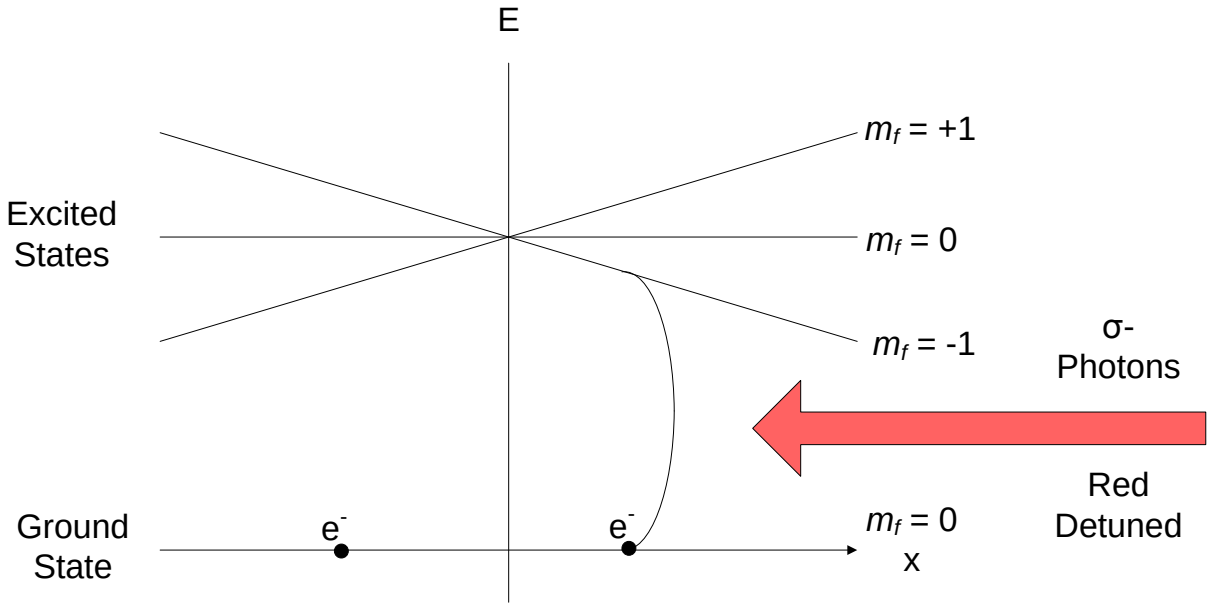

Figure 2-5 - Zeeman splitting and circularly polarized photons exert a central force on atoms in a MOT.

Due to the linear Zeeman effect, the degeneracy of hyperfine transitions is lifted. Due to momentum conservation laws different states can only accept photons that carry positive or negative

angular momentum. σ^- photons carry negative spin angular momentum and so the total angular momentum is conserved if the electron transitions to a negative angular momentum state. For electrons on the other side of the origin, a laser with σ^+ photons will be absorbed. If light polarization is chosen appropriately for all lasers in a MOT, then photons will feel a force that towards the origin of the MOT. In this way atoms can be collected and prepared for a dipole trap.

3.1.2 Dipole Traps

The dipole traps are the most important feature of this experiment because they are responsible for controlling the positions of the atoms and allow for addressability while performing operations on qubits. These dipole traps are also unique because they have never before been demonstrated.

3.1.2.A Dipole – Laser Interaction Potential Energy

Dipole traps or far-off resonance traps (FORTs) take advantage of the interaction between electromagnetic fields and the induced dipole of an atom for trapping. The following section gives an overview of this interaction (see Grimm's paper[10] for more information on this phenomenon). Equation (2-4) defines the induced dipole $\vec{p}$ of an atom by an electric field $\vec{E}$.

$$\vec{p} = \alpha\vec{E} \tag{2-4}$$

In (2-4) α is the complex polarizability of the atom due to the electric field $\vec{E}$. The potential energy U_{dip} of the atom with an induced dipole in this field is then given by (2-5) if the electric field is sinusoidal.

$$U_{dip} = -\frac{1}{2} < \vec{p} \cdot \vec{E} >= -\frac{1}{2\varepsilon_o c} Re(\alpha) I \tag{2-5}$$

In equation (2-5), ε_o is the permittivity of free space, c is the speed of light, the <> operator denotes a time averaging, and I represents the intensity of the electric field. The force of this interaction F_{dip} is then given by (2-6).

$$F_{dip} = -\vec{\nabla} U_{dip} = \frac{1}{2\varepsilon_o c} Re(\alpha) \vec{\nabla} I(r) \tag{2-6}$$

In equation (2-6), the interaction force F_{dip} is restorative in the maximum intensity points of the electric field if $Re(\alpha)$ is positive and in the minimum intensity points of the electric field if $Re(\alpha)$ is negative. An approximation of $Re(\alpha)$ for far detuned lasers is given in (2-7)[11].

$$Re(\alpha) = \frac{\alpha_o}{\omega_o^2 - \omega^2} \tag{2-7}$$

In equation (2-7) α_o represents the real portion of the complex polarizability when the electric field's frequency is far from resonance (e.g. $h \cdot 0.1340 \frac{Hz}{\left(\frac{V}{cm}\right)^2}$ for the cycling transition in ^{87}RB according to Steck[11]). For a more detailed derivation of the induced dipole potential energy, the force the atom experiences from the dipole trap, or the polarizability constant see a book Gillen et al.[12]. Figure 2-6 shows this function plotted for $\omega_o = 2\pi\ 385\ \text{THz}$ (^{85}RB $5S_{1/2} \rightarrow 5P_{3/2}$ transition).

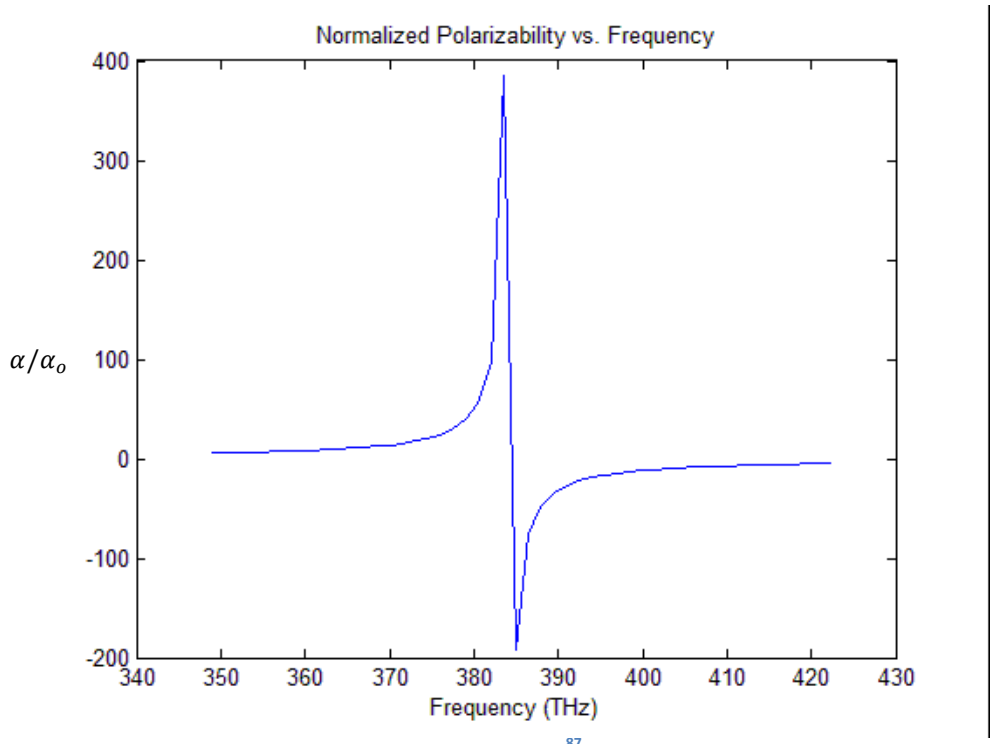

Figure 2-6 - Normalized polarizability of ^{87}Rb vs. laser frequency.

Due to the results of Figure 2-6, red-detuned lasers will cause atoms to be trapped in their bright spots and blue-detuned lasers will cause atoms to be trapped in their dark spots.

3.1.2.C Dipole Trap Projection

The issue with the dipole traps used in this setup is that they only appear in the diffraction pattern of a laser immediately behind a pin-hole. This makes it difficult to place the traps into the MOT where they will trap cooled ^{87}Rb atoms. In order to fix this issue, the traps are projected into the MOT using the setup in Figure 2-7.

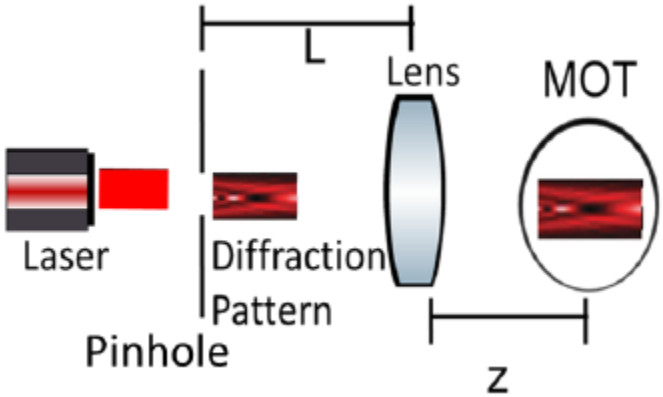

Figure 2-7 - Dipole trap projection diagram[13].

In this way, the size and location of the traps can be controlled. Once the traps can be created and projected into a MOT, atoms can be transferred from a MOT to the dipole traps, and the following section covers methods for how to do that.

2.2 Successful Transfer Techniques

Our project, to date, has successfully built at MOT and trapped ^{87}Rb. The goal of this project is to test pinhole diffraction patterns as a scalable quantum computing technology. To do this, the ^{87}Rb atoms must be transferred from the MOT to the traps generated by our pinhole diffraction patterns. There have been several different approaches to transfer trapped atoms from a MOT to optical dipole traps. This paper discusses three such approaches and their experimental requirements, with the goal of understanding which components our project will require.

The first approach discussed in this paper was carried out by Wieman's group[14] in 2000. Their group transferred ^{85}Rb atoms from a MOT to a far off-resonance trap (FORT). Their group used a home-built titanium sapphire laser focused through a doublet lens to generate the FORT. The FORT laser's wavelength was red detuned by 2-4 nm. Their group then transferred approximately 8 X 10^6 atoms into their FORT using the following steps:

1) Fill MOT for approximately 3 s with maximum MOT repump laser intensity
2) Switch FORT on while increasing the detuning of the MOT and decreasing the repump intensity for 20-200 ms
3) Deactivate the MOT laser, MOT repump laser, and magnetic fields after ~100 ms

The second transfer approach considered in this paper was performed by Thomas's group[15] in 2001. While their group used CO_2 laser Quasielectrostatic traps (QUESTs) instead of FORTs, the group did have success in verifying their model for trap loading dynamics. They were able to transfer 4 X 10^5 atoms into their QUESTs using the following steps:

1) First load the MOT for 3 s
2) Further cool the MOT by tuning the MOT lasers closer to resonance while reducing their intensity for up to 30 ms
3) Allow QUESTs to come into thermal equilibrium with MOT for ~4 ms

The third approach considered in this paper was performed by Han et al.[16] in 2001. This group used Cs atoms instead of ^{85}Rb, but was able to trap 3 X 10^7 atoms their dipole traps. This process is more experimentally complex than the other two approaches discussed. They follow the steps shown below:

1) The MOT is first loaded.
2) The MOT and repump laser intensities are lowered
3) The MOT laser is further detuned 5 ms after the laser intensities are decreased
4) The magnetic field intensity is increased 5 ms later
5) At peak MOT density, the atoms are transferred into a 1-D far off-resonance lattice (FORL), which is then converted into a 3-D FORL
6) The atoms are then pumped into their lowest energy state and are adiabatically released
7) The atoms are then finally magnetically levitated and transferred to their final FORT

The primary reason for why this approach will not be considered in current system design, is due to the extra FORL required by the transfer process. The current lab setup doesn't have the ability or

room to add an extra 3-D FORL. This technique is important to keep in mind as the project grows in its capabilities as a possible option for a future transfer mechanism.

The general steps required for a MOT to dipole trap transfer are: 1) load atoms to MOT, 2) adjust MOT parameters (laser intensities, detuning, and magnetic field) to increase atom density, 3) deactivate MOT and allow majority of atoms to be trapped inside activated dipole trap.

2.3 Dipole Measurement Technique

To perform quantum computations on neutral atoms in dipole traps, the strength and shape of those dipole traps must be well known. The property used to quantify the "tightness" of the dipole trap is the trap frequency. The dipole trap is modeled as a simple harmonic oscillator with $U_{dip} = \frac{1}{2}m\omega^2x^2$. The trap frequency is then $f = \frac{\omega}{2\pi}$. The technique discussed in this paper for characterizing dipole trap resonant frequencies was described by Havey's group[17]. In their experimental setup, they transferred ^{87}Rb atoms from a MOT to a CO_2 QUEST before parametrically driving the QUEST at different frequencies to determine the QUEST resonant frequencies. Their experimental process for driving a QUEST parametrically is listed below.

1) Atoms are loaded from the MOT to the QUEST.
2) QUEST intensity is modulated at a certain frequency for specified period of time.
3) QUEST is turned off and atoms are allowed to expand for 3 ms.
4) Atom cloud density is observed.
5) At a modulation frequency of twice the trap frequency, a significant decrease in the atom cloud density is seen.

2.4 System Requirements

Based on the techniques discussed for transferring atoms from a MOT to a dipole trap and for characterizing the resonant frequency of a dipole trap, Table 2-1 lists required optical and magnetic system control specifications.

Table 2-1 - Required Optical and Magnetic System Specifications

Optical System Requirements	
Specification	Value
Laser Amplitude On/Off Switching Duration	~1 ms
Laser Frequency Switching Duration	~1 ms
Laser Amplitude Modulation On/Off Switching Duration	~100 µs
Laser Amplitude Reduction Duration	~1 ms
Magnetic System Requirements	
Magnetic Amplitude On/Off Switching Duration	~1 ms

3: Required Components

Currently, a working MOT has been assembled for this project. The next phase of the project requires the transfer of the atoms from the MOT to dipole traps for the purpose of performing quantum computing. In their experiments, Wieman[14] and Thomas [15] implement precise and fast control of their MOT lasers, FORT/QUEST lasers, and MOT magnetic fields. To do that for this lab setup, the DIO 64 will be used. The DIO 64 is a digital input/output board that can be controlled with a LabVIEW program. The goal of this project was to evaluate and modify the systems in place to attain the same level of precise high speed control for our atom traps.

3.1 Magnetic Coil Control System

The magnetic coil controls system must switch the magnetic fields on and off. Furthermore, the control of the fields must be fast (the field must be switched off on the order of ~1 ms). Figure 3-1 displays the uncontrolled magnetic coil setup.

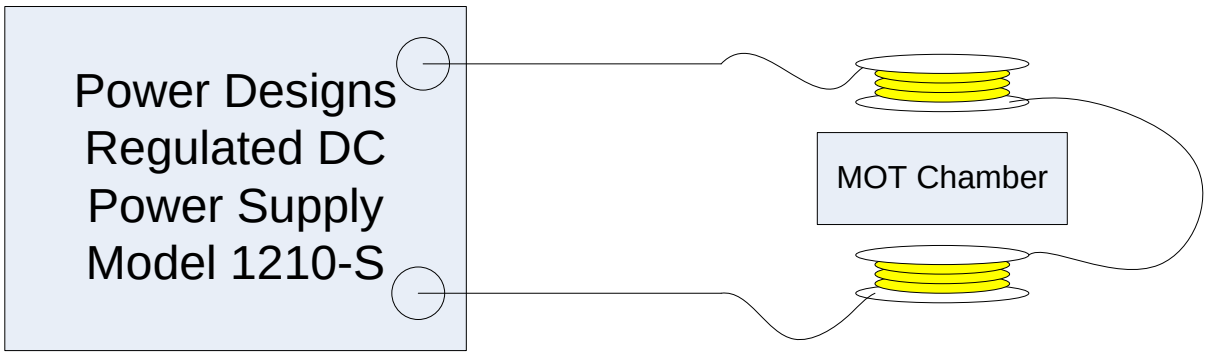

Figure 3-1 - MOT coil setup block diagram.

The control circuitry needs to impede current through the coils. Figure 3-2 depicts where the circuitry should be placed to accomplish this goal.

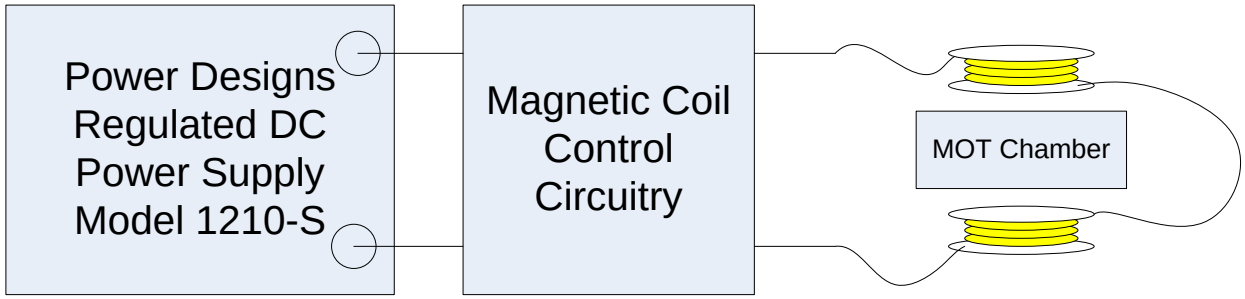

Figure 3-2 - MOT coil setup with added control circuitry block diagram.

The requirements for this circuitry are that it can be placed in between the power supply and the MOT coils easily and that it can switch the current of the MOT chamber off in less than ~1 ms. The magnetic coil control circuitry's circuit diagram can be found in Appendix A and the circuit's test results are discussed in Chapter 4.

3.2 Optical Control Systems

The control system for this project's MOT and dipole trap lasers will be a mixture of purchased and designed components as it was for the magnetic coil control system. The purchased and already designed components consist of acousto-optical modulators (AOMs), AOM signal generators, mechanical shutters, and dichroic atomic vapor laser locks (DAVLLs).

4.2.1 Laser Amplitude On/Off Switching

To maintain laser frequency stability, the actual laser diode is not manipulated when a laser beam needs to be switched off. The beam is only deflected or blocked. An AOM and mechanical shutter are combined to achieve this switching at high speed. The AOM controls the majority of the laser power with high speed optical diffraction. The mechanical shutter completely blocks the optical beam but at a slower rate. When these two systems are used in conjunction, complete optical on/off switching can be achieved. Both the AOMs and the mechanical shutters were characterized for this project and their measurements are displayed in Appendix B and Appendix C respectively.

4.2.2 Laser Amplitude Control

With proper alignment, the AOM crystals can be used to only diffract a desired amount of optical power(maximum optical power diffraction is ~80%) and thus control the laser amplitude. In this way, there is digital control laser amplitude reduction by a preset amount. This preset amount is determined by controlling the alignment of the AOM. The AOM is digitally controlled by applying a 0-5 V signal to the digital signal port.

4.2.3 Laser Frequency Control

The current setup for stabilizing the project's laser frequencies involves the use of a DAVLL. The DAVLL is a negative feedback control system where the plant is the laser diode and the output is the laser frequency. The laser frequencies are measured by exposing them to ^{87}Rb atoms in a magnetic field. The atoms experience a Zeeman splitting and as a result absorb different amounts of left and right circularly polarized light based on the frequency of the photons they see. Any change in the ratio of polarization intensities is measured and represents any change in the laser frequencies which is compensated by adjusting the laser's output frequency. This project's DAVLL was custom built[18].

Due to the topology of this circuit, signals can be injected into the control circuitry to shift the laser's frequencies. In this way, necessary laser frequency shifts can be obtained. The performance of this system wasn't measured for this paper and should be measured in the future.

4.2.4 Laser Amplitude Modulation On/Off Switching

The dipole trap laser amplitudes must be modulated in order to properly characterize their resonant frequencies. The AOM function generators have a digital input to control the on/off state of the AOM and an analog input to generate amplitude modulation. In the lab there is a sine wave generator that can drive the analog input to the AOM signal generator as shown in Figure 3-3.

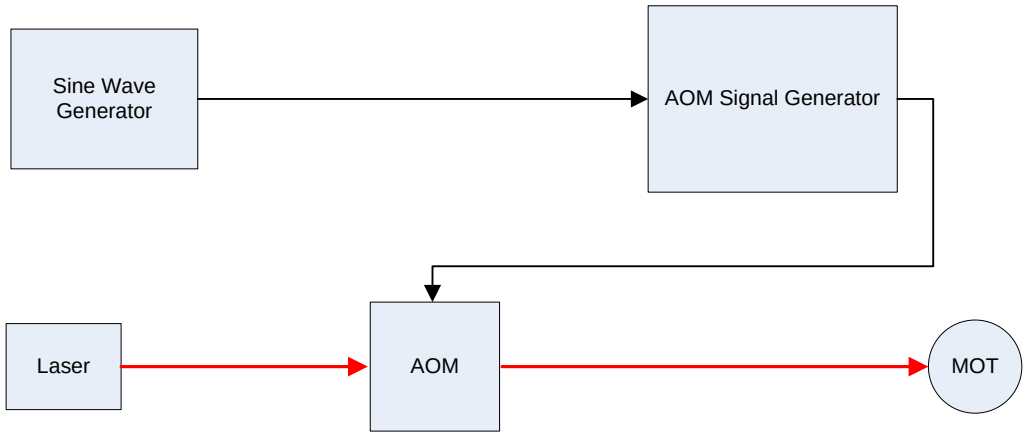

Figure 3-3 - Laser amplitude modulation setup with no controller.

To introduce digital control of the amplitude modulation into the system while maintaining the AOM on state, a circuit should be introduced between the sine wave generator and the AOM signal generator. The circuit would have to have a switching time of ~1 ms and be able to handle at most 1 Vpp signals as per the AOM signal generator specifications. The resulting system would resemble that shown in Figure 3-4.

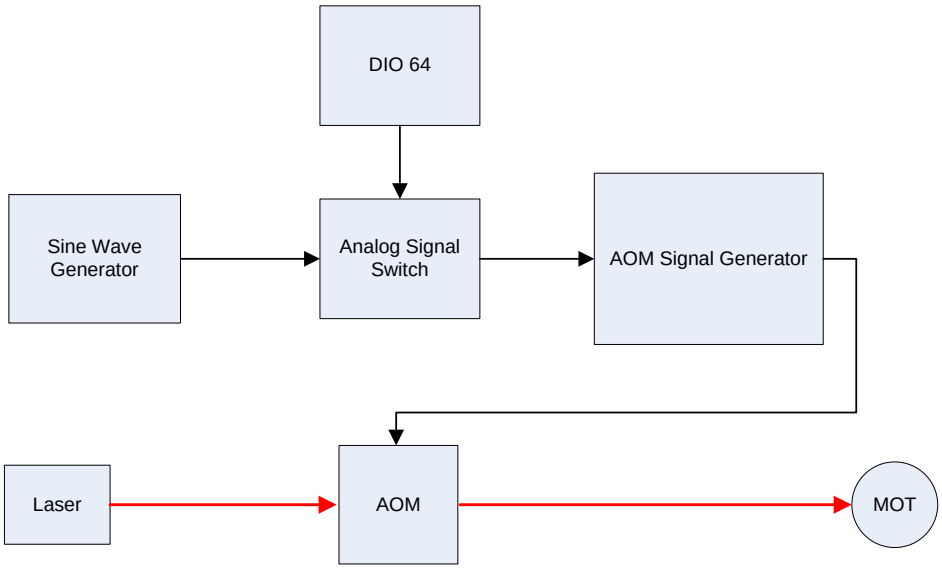

Figure 3-4 - AOM modulation setup with added control component.

This circuit must be properly terminated to maintain 50 Ω terminations at the AOM signal generator due to the existence of high frequency high power signals that can be coupled to the analog port of the device. The analog signal switch's circuit diagram is shown in Appendix D and the circuit's test results are discussed in Chapter 5.

4: Magnetic Coil Switch

The magnetic coils for the MOT have to generate a quadrupole magnetic field with a large gradient and so large currents (>1 A) are required. To properly design a circuit that can switch this amount of current quickly, the parameters of the magnetic coils must be measured first.

4.1 Magnetic Coil Switch Design

To properly design the circuit that will be controlling the coil current, the coils must be modeled and characterized. Once the magnetic coils are measured, components can be selected to properly regulate the magnetic coil currents.

5.1.1 Modeling Magnetic Coils

Electromagnetic coils are meant to create magnetic fields. For this project, the larger the current through the coils the stronger the magnetic field gradients generated by them. The problem with turning off a magnetic field quickly is that due to Maxwell's equations, the electric field becomes intense due to a rapidly changing magnetic field.

When designing circuits, it is convenient to deal with voltages and currents instead of electromagnetic fields. To do this, magnetic coils must be modeled as an inductor. Equation (4-1) defines the voltage-current relationship for an inductor.

$$V_C = L_C \frac{dI_C}{dt} \tag{4-1}$$

V_C is the voltage across the magnetic coil, L_C is the coil inductance, and $\frac{dI_C}{dt}$ is the rate of change of the current through the inductor. To change the current through the magnetic coils quickly will generate a large voltage according to (4-1). Large voltages in a circuit can break components so the magnetic coil inductance must be measured before component selection can be performed.

5.1.2 Measuring the Magnetic Coils

The magnetic coil inductances were measured using the setup shown in Figure 4-1.

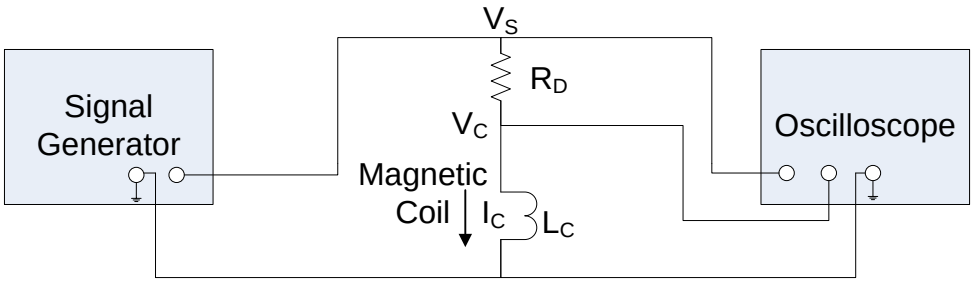

Figure 4-1 - Magnetic coil inductance measurement setup.

A 1 V sinusoid at different frequencies f was presented from the signal generator, and the resulting voltage across the inductor was measured.

5.1.3 Coil Inductance Measurement Results

Based on the circuit shown in Figure 4-1, the resulting relationship between $|V_C|$ and $|V_S|$ is given by (4-2). The equation shown in figure (4-2) is the result of a LC high pass filter topology and the derivation for such a circuit can be found in Tooley et al[19].

$$\left|\frac{V_C}{V_S}\right| = \frac{2\pi f L_C}{\sqrt{R^2+(2\pi f L_C)^2}} \tag{4-2}$$

The impedance of an inductor increases as the frequency of the sinusoid increases. It is this behavior that makes it difficult to adjust the current through an inductor quickly. Equation (4-3) displays the relationship for L_C given the ratio $\left|\frac{V_C}{V_S}\right|$.

$$L_C = \frac{\left|\frac{V_C}{V_S}\right| R}{2\pi f \sqrt{1-\left|\frac{V_C}{V_S}\right|^2}} \tag{4-3}$$

The recorded gain $\left|\frac{V_C}{V_S}\right|$ at measured angular frequencies (rad/s) is shown in Table 4-1 along with the corresponding calculated L_C.

Table 4-1 - Measured coil inductance.

Gain	ω (rad/s)	L_C (mH)
0.031	1240	24.9
0.076	3100	24.3
0.151	6350	22.9
0.297	12600	20.9
	Average L_C (mH)	23.2

Based on the measured coil inductance of Table 4-1, and the desired switching time of <1 ms, the design of Appendix A was chosen.

4.2 Magnetic Coil Switch Test

The circuit shown in Appendix A is connected to the antiparallel Helmholtz coils surrounding the MOT chamber as shown in Figure 4-2.

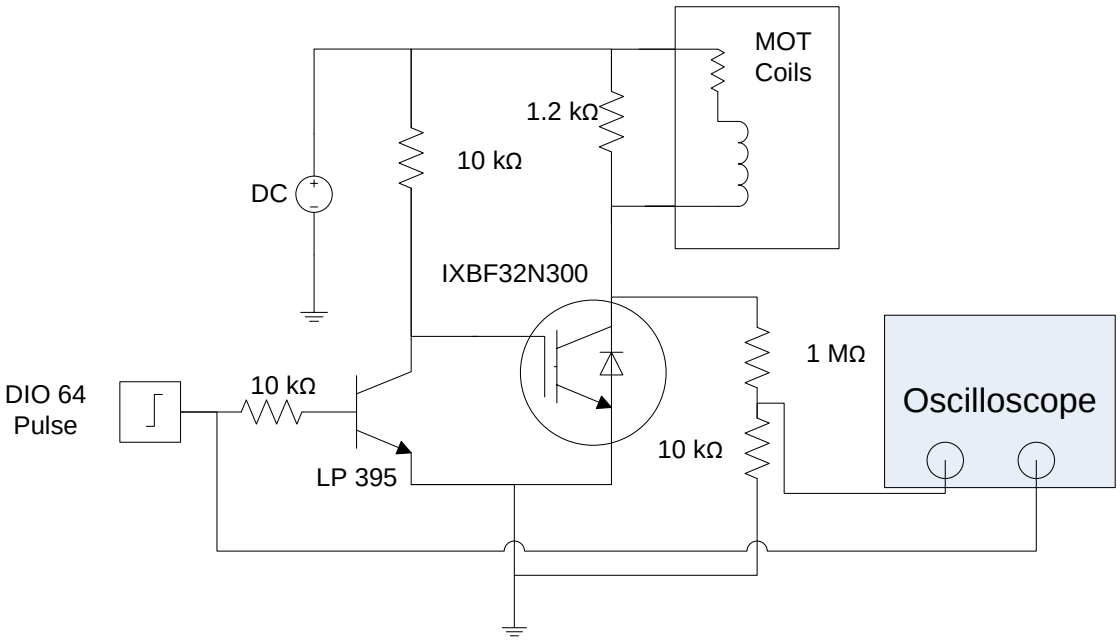

Figure 4-2 - Test setup for MOT magnetic field switch.

The oscilloscope triggers off of the DIO 64 control signal and measures the voltage across the IXBF32N300 insulated gate bipolar transistor (IGBT). The 1.01 MΩ voltage divider, connecting the IGBT and the oscilloscope, attenuates the signal to approximately 1/100 of the actual value. Its value is large enough that it also avoids loading so that the system operates as if the resistors were not there. Only the rising edge of the DIO 64 control signal is of importance as that edge is what determines the speed and timing of when the current through the coils is switched off.

4.3 Results

The circuit in Figure 4-2 was measured by first varying the drain resistance (depicted as the 1.2 kΩ resistor). The current through the coils was switched off at three resistance values and the voltage across the IGBT was observed. Figure 4-3 depicts the voltage curve across the IGBT with a drain resistance of 750 Ω.

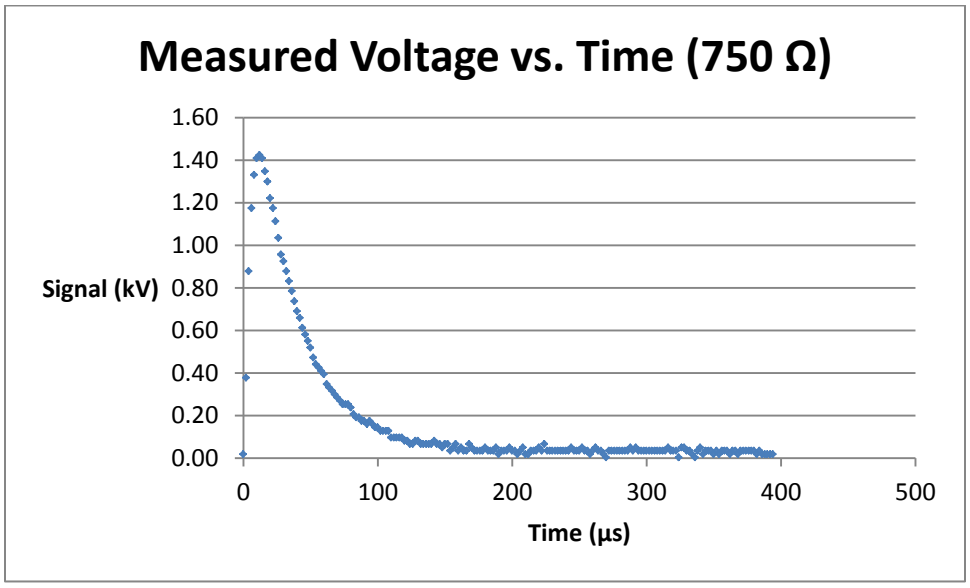

Figure 4-3 - Discharge curve of magnetic coils with a drain resistance of 750 Ω.

The discharge curve represents the voltage across the IGBT. Figure 4-4 shows a simplified circuit model of the magnetic coil switch for analysis.

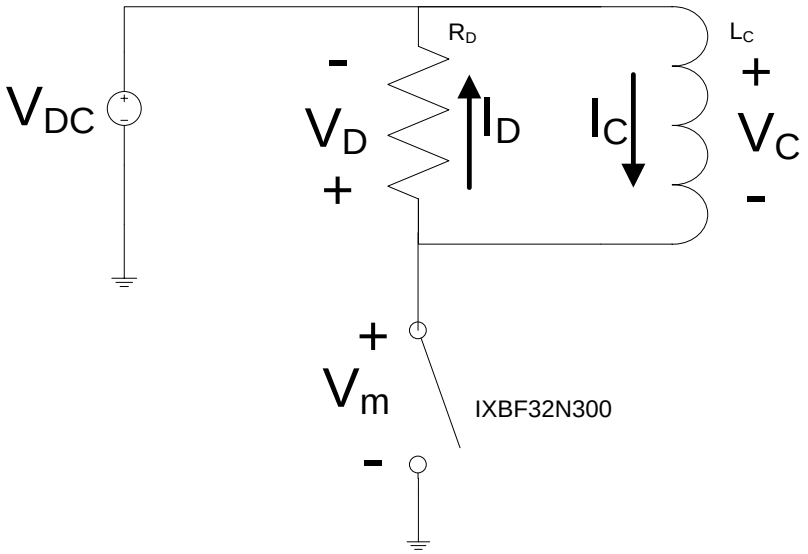

Figure 4-4 - Simplified circuit model of the magnetic coil switch circuit.

V_m represents the measured voltage shown in Figure 4-3. Equation (4-4) gives an expression for the measured voltage in terms of the drain resistor voltage V_D and the rail voltage V_{DC}.

$$V_m = V_{DC} + V_D \tag{4-4}$$

According to Figure 4-3, V_D is on the order of kV and it is known that V_{DC} is on the order of 10V so equation (4-4) can be approximated by equation (4-5).

$$V_m \approx V_D \tag{4-5}$$

According to Kirchhoff's voltage and current laws, the voltages and currents of the drain resistor R_D and the coil inductor L_C are related by equations (4-6) and (4-7) once the IXBF32N300 IGBT switch is turned off.

$$V_D = -V_C \tag{4-6}$$

$$I_D = I_C \tag{4-7}$$

Combining equations (4-1), (4-6), (4-7), and Ohm's Law yield yields the differential equation shown in (4-8).

$$\frac{dV_D}{dt} = \frac{-L_C}{R_D} V_D \tag{4-8}$$

Solving equation (4-8) yields equations (4-9), (4-10), and (4-11) for the voltage through the resistor once the IGBT switch is shut off.

$$V_D(t) = V_o e^{\frac{-t}{\tau}} \tag{4-9}$$

$$V_o = I_o R_D \tag{4-10}$$

$$\tau = \frac{L_C}{R_D} \tag{4-11}$$

In equation (4-10), I_o is the current through the magnetic coils as the IBGT is switched off. Combining equations (4-5) and (4-8) yields (4-12), an equation for the curve shown in Figure 4-3.

$$V_m(t) = V_o e^{\frac{-t}{\tau}} \tag{4-12}$$

The exponential decay of the measured voltage was tabulated for 3 different drain resistances and the resultant τ values are displayed in Table 4-2. It is important to note that equation (4-12) only describes the rate at which the voltage across the coils decreases. The voltage across the coils doesn't

instantly reach its maximum within the first 20 µs because the IGBT doesn't turn off instantly, due to the current limitations of the LP 395.

Table 4-2 - Coil Calculations for Varied Drain Resistance

$\tau\ (\mu s)$	$R_D(\Omega)$	L_C (mH)
37.4	750	28.1
28.7	1000	28.7
27.0	1200	32.37
	Average L_C	29.7

4.4 Magnetic Coil Switch Discussion

By observation, the discharge curves of the current through the MOT magnetic coils were exponential as predicted. The inductance measurements of the coil at low currents and the resulting inductance measurements from the magnetic coil switch measurements varied by approximately 20 %. In this way, the model of an inductor proved to be relatively accurate for the design of a current switch. For an exponential decay circuit, the signal reaches 5 % of its original magnitude after 3τ. The resulting switching speed is then 81 µs for the drain resistance of 1200Ω. Another way to decrease the switching duration would be to swap the LP 395 with a higher current BJT or MOSFET. A MOSFET would remove the need for the 10 kΩ resistor at the base of the LP 395.

5: AOM Modulation Switch

The AOM modulation signal will be used to test the dipole trap resonance frequencies. In order to properly measure the system before and after modulation, the AOM must remain active while the modulation to the AOM signal is switched on and off quickly.

5.1 AOM Modulation Switch Design

During the resonance measurement, modulation will be tested at many different frequencies. Due to this requirement, the switch must be able to handle a variety of frequencies from 0 Hz to 1 MHz. To accomplish this, a single pull double throw (SPDT) analog switch IC (ADG918) was chosen. The complete circuit diagram and board layout can be found in Appendix D.

The biasing was accomplished with batteries and diodes. The batteries were chosen to bias the switch so that the device would be more portable and so that a new power supply wouldn't need to be purchased by the group. Diodes were preferred to drop the battery supplies down to the proper level due to their tendency to maintain constant voltage drops over larger current ranges.

5.2 AOM Modulation Switch Testing

The setup shown in Figure 5-1 was used to measure the steady-state performance of the analog switch during modulation and how the switch is impeded the sine wave generator.

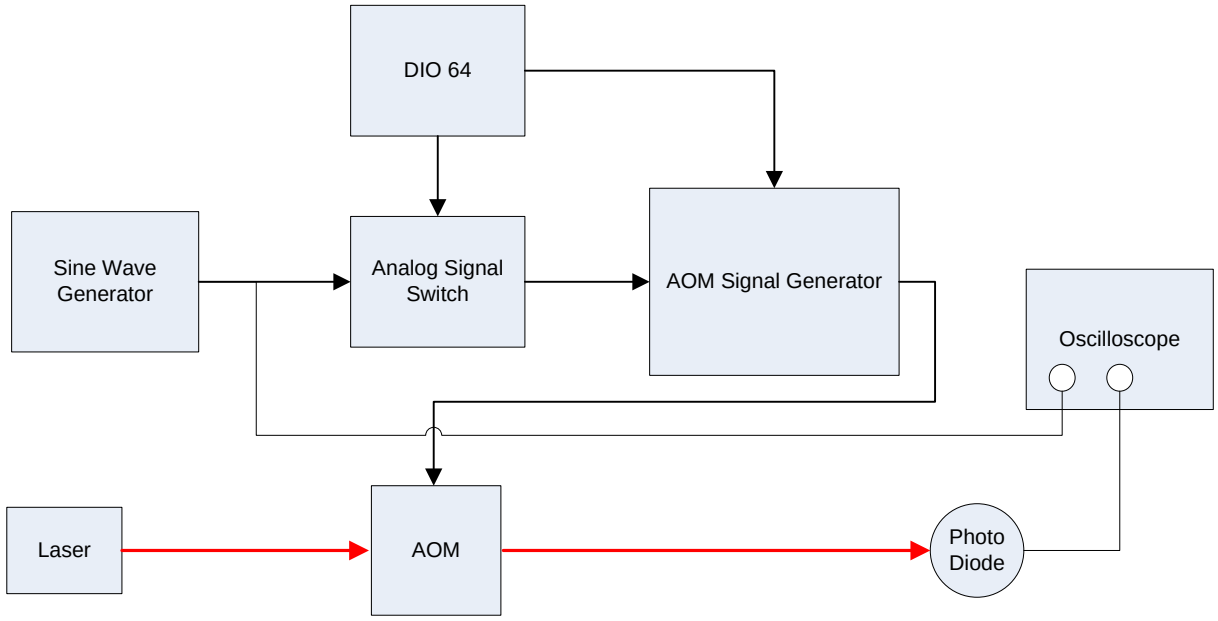

Figure 5-1 - Analog modulation switch steady state test setup.

Figure 5-2 displays the results of the modulation signal while the switch is on.

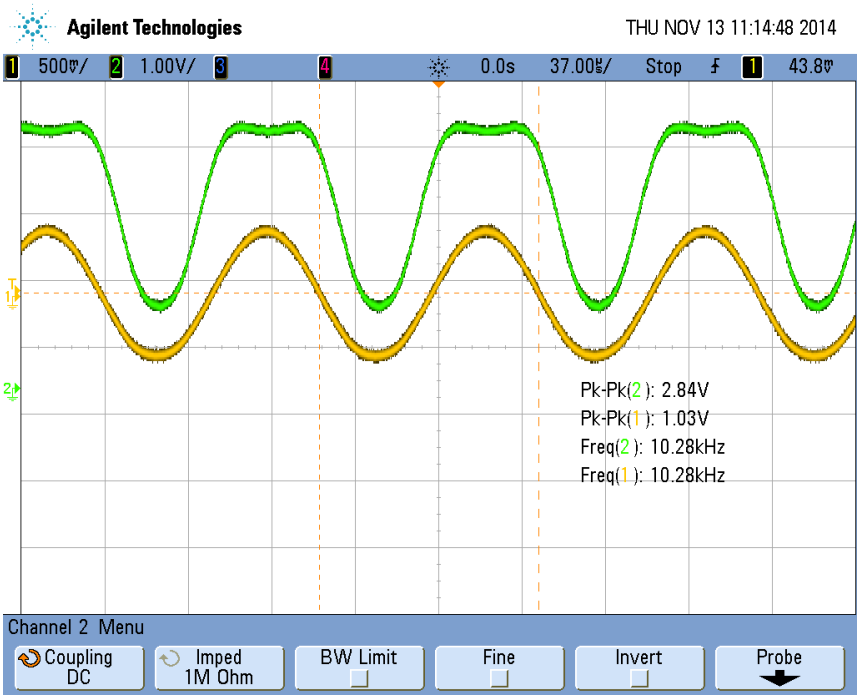

Figure 5-2 - AOM Modulation. The yellow (bottom) waveform is the modulation signal and the green (top) waveform is the AOM diffracted laser intensity.

Figure 5-3 displays the measured AOM modulation while the switch is impeding the sine wave generator from driving the AOM signal generator.

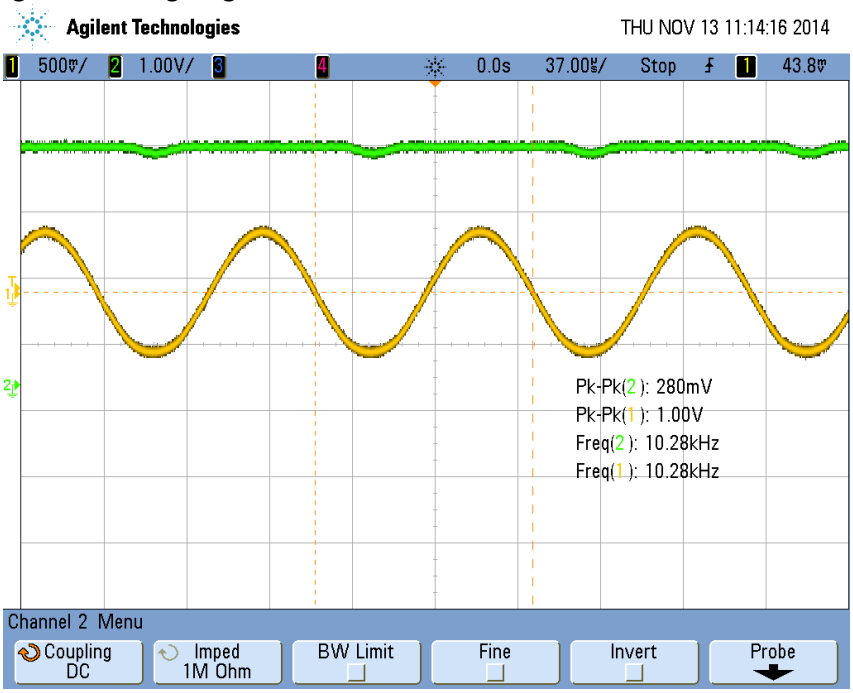

Figure 5-3 – AOM switch isolation. The yellow waveform (bottom) is the modulation signal and the green (top) waveform is the AOM diffracted laser intensity.

Some of the signal still affects the AOM diffraction but it is only modulated by 5.95 % of its diffraction intensity whereas the modulation intensity while the switch is on reaches 70.6%. Equation (5-1) displays the equation used to calculate the modulation percentage.

$$Modulation\ Percentage = \frac{Signal\ \text{Maximum} - \text{Signal Minimum}}{\text{Signal Maximum}} 100\% \quad (5\text{-}1)$$

To measure the switching speed of the AOM modulation switch, the setup shown in Figure 5-4 was used. The DIO 64 signal was sent to the oscilloscope as a trigger to directly capture the AOM switch circuit's switching characteristic (voltage vs. time curve).

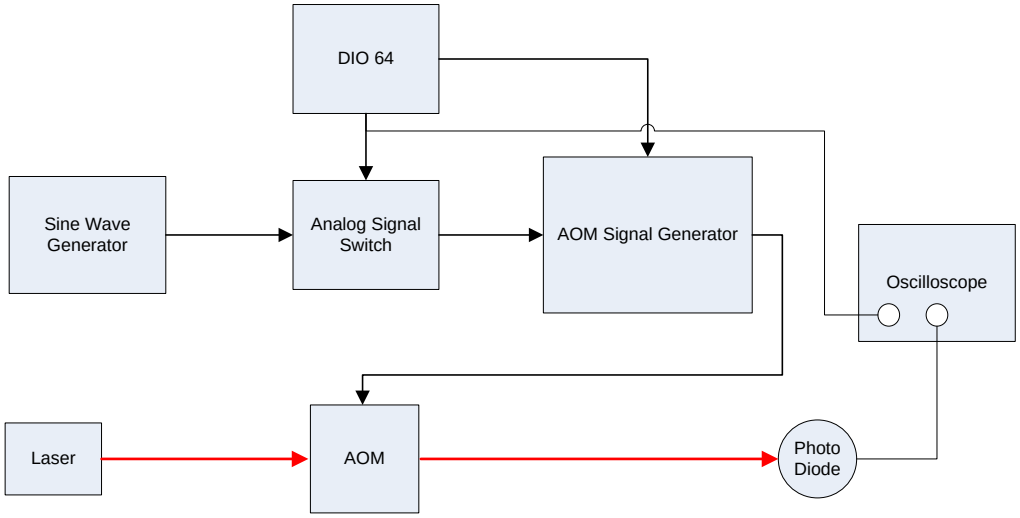

Figure 5-4 - AOM modulation switching speed test setup.

The waveform shown in Figure 5-5 displays the test results of the AOM modulation switch's speed.

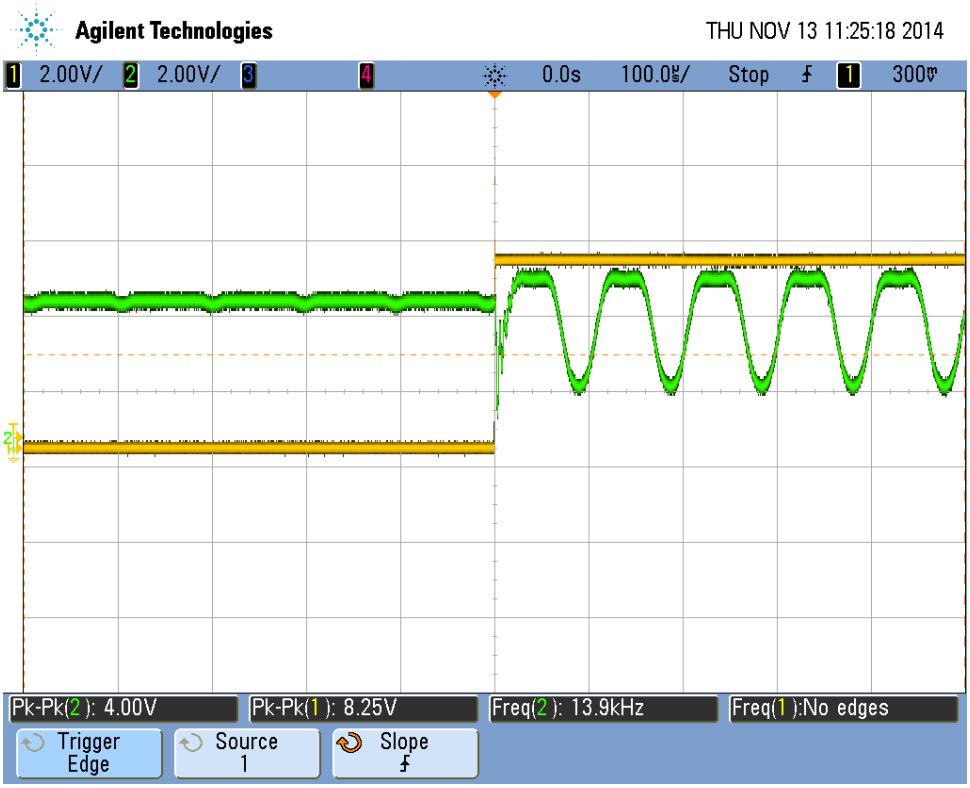

Figure 5-5 - Oscilloscope capture of the AOM modulation switch from off to on. The yellow waveform (square pulse) is the DIO 64 trigger signal and the green waveform (varying curve) is the diffracted AOM laser intensity.

The measured switching time of the AOM modulation switch was measured to be ~25 µs which is faster than the specified ~100 µs. The switch can handle signals within ± 0.5 V, before attenuating them. This will provide some protection to the AOMs from damage. The AOMs can be damaged if the function generator modulation signal intensity is too large. That being said, the signal being fed into the AOM modulation switch should always be within ± 0.5 V.

5.3 AOM Modulation Switch Discussion

The overall switch design was fairly simple with the majority of the switching circuitry being contained within the ADG918 IC. The circuit does have a switching time of approximately ~25 µs. Previous results calculated radial resonance frequencies of ~90 kHz and axial resonance frequencies of ~ 10 kHz[7]. This switching time shouldn't hinder experimental progress for this project because it is of the same order as the desired resonant frequencies. Overall, this switch should perform sufficiently to accurately measure dipole trap resonant frequencies based on the considerations discussed.

6: Conclusion

The goal of this project was to contribute to the transfer sequence between a MOT and pinhole dipole traps for the purpose of neutral atom quantum computing and to contribute to the characterization of those pinhole dipole traps. A magnetic field switch and AOM switch were designed and AOMs, mechanical shutters, were characterized for the transfer process. All of the components tested performed the desired functions for future work to proceed to dipole trap testing. Therefore nothing stands in the way of the transfer of the atoms from a MOT to the pinhole traps and the characterization of those traps for future quantum operations.

7: Bibliography

[1] P.W. Shor, "Polynomial time algorithms for prime factorization and discrete logarithms on a quantum computer," SIAM J. Comput. 26 1484 (1997).

[2] David P. DiVincenzo, "The Physical Implementation of Quantum Computation," Fortschr. Phys. 48, 771-783 (2000).

[3] L. M. Vandersypen, M. Steffen, G. Breyta, C. S. Yannoni, M. H. Sherwood, and I. L. Chuang, " Experimental realization of Shor's quantum factoring algorithm using nuclear magnetic resonance," Nature 414(6866), 883-887 (2001).

[4] I. Marcikic, H. D. Riedmatten, W. Tittel, V. Scarani, H. Zbinden, and N. Gisin, "Femtosecond Time-Bin Entangled Qubits for Quantum Communication," Phys. Rev. A 66, 062308 (2002).

[5] T. Monz, P. Schindler, J. T. Barreiro, M. Chwalla, D. Nigg, W. A. Coish, M. Harlander, W. Haensel, H. Hennrich, and R. Blatt, "14-qubit entanglement: creation and coherence," Phys. Rev. Lett. 106, 130506 (2011).

[6] M. Saffman, T. G. Walker, and K. Mølmer, "Quantum information with Rydberg atoms," Rev. Mod. Phys. 82, 2313 (2010).

[7] B. D. Copsey and K. Gillen-Christandl, "Polarization-dependent atomic dipole traps behind a circular aperture for neutral atom quantum computing," Phys. Rev. A 83, 023408 (2011).

[8] G. D. Gillen, S. Guha, and K. Gillen-Christandl, "Optical dipole traps for cold atoms using diffracted laser light," Phys. Rev. A 73, 013409 (2006).

[9] K. Gillen-Christandl and G. D. Gillen, "Projection of diffraction patterns for use in cold-neutral atom trapping," Phys. Rev. A 82, 063420 (2010).

[10] R. Grimm, M. Weidemuller, and Y. B. Ovchinnikov, "Optical Dipole Traps For Neutral Atoms," Adv. At. Mol. Opt. Phys. 42, 95 (2000).

[11]D. A. Steck, "Rubidium 87 D line data," (2001).

[12] Glen D. Gillen, Katharina Gillen, and Shekhar Guha, Light Propagation in Linear Optical Media, (CRC Press, Taylor & Francis Group, Boca Raton, FL 2014), Section 11.2.

[13]Sanjay Khatri, Senior Project, California Polytechnic University, San Luis Obispo, 2014.

[14]S. J. M. Kuppens, K. L. Corwin, K. W. Miller, T. E. Chupp, and C. E. Wieman, "Loading an optical dipole trap," Phys. Rev. A 62, 013406 (2000).

[15]K. M. O'Hara, S. R. Granade, M. E. Gehm, and J. E. Thomas, "Loading dynamics of CO_2 laser traps," Phys. Rev. A 63(4), 043403 (2001).

[16]D. J. Han, M. T. DePue, and D. S. Weiss, "Loading and compressing Cs atoms in a very far-off-resonant light trap," Phys. Rev. A 63(2), 023405 (2001).

[17] S. Balik, A. L. Win, and M. D. Havey, "Image-based parametric resonance in an optical dipole-atom trap," Phys. Rev. A 80(2), 023404 (2009).

[18] Eric S. Muckley, Senior Project, California Polytechnic University, San Luis Obispo, 2009.

[19] M. Tooley and M. H. Tooley, Electronic circuits: fundamentals and applications. (Routledge, 2006).

8: Appendix

A. Magnetic Coil Switch

Table 8-1 shows a list of the various components used in the magnetic coils switch along with their prices, quantity, and purpose within the circuit.

Table 8-1- Magnetic coil switch parts list

Part Number	Part Description	Quantity	Purpose	Unit Price
LP395	Power transistor made by Texas Instruments	1	Translate the DIO 64 digital control signal level to a signal level that can drive the IGBT.	$1.56
PWR221T	50 Ω 30 W power resistor manufactured by Bourns.	30	To assemble a 1.2 kΩ drain resistor to dissipate the energy stored in the magnetic coils.	$2.17
IXBF32N300	Power IGBT manufactured by IXYS.	1	To switch direct the current through the drain resistor or through the power supply. This component acts as a buffer between the coil voltage spikes and the power supply.	$55.32
10 K	Standard 10 kΩ resistor	2	To bias the LP395 BJT digital signal translator.	$0.10
Banana Plug	Standard female banana plug	5	To connect external signals to this circuit.	$1.84
Wire	5 feet of 16 gauge solid core wire	1	To handle large circuit currents.	$0.00
Total Cost				$131.38

Figure 8-1 displays the magnetic coil switch circuit diagram assembled using the parts given in Table 8-1.

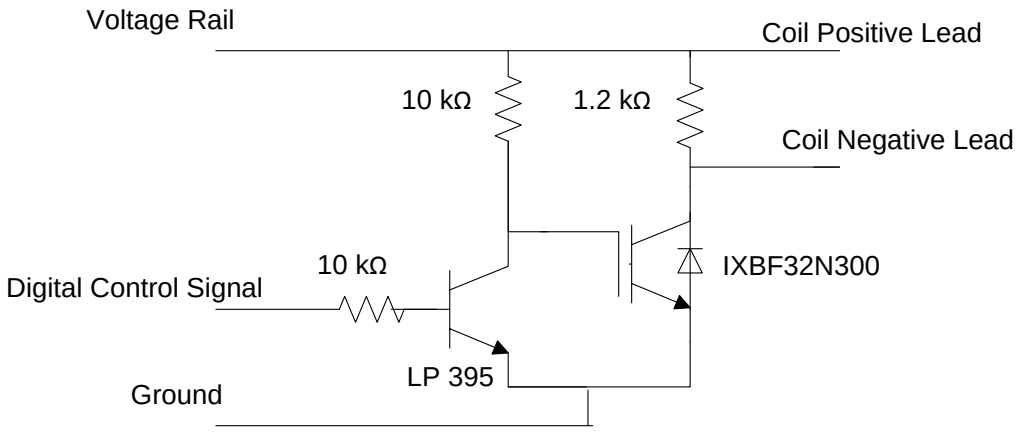

Figure 8-1 - Magnetic coil switch circuit schematic.

B. Acousto-Optical Modulators (AOMs)

The AOMs used in our lab are IntraAction Model AOM-402AF3 modulators. They allow for high speed control of the laser intensity, but do not deflect all of the optical power. AOMs function by taking advantage of the coupling between acoustic vibrations in a crystal and the optical properties of that same crystal. In an AOM, mechanical waves cause local expansion and compression within a crystal, resulting in a periodically changing refractive index of the crystal. These areas allow for a form of Bragg diffraction to occur. As a result, a large percentage of the optical power that would usually travel through the crystal unhindered is diffracted. In this way, high speed control of the optical power of a laser can be achieved.

B.1 Test Setup

The AOMs are driven by an IntraAction Model ME-403H6 Light Modulator Signal Processor. There are three pairs of AOM/Processors in the lab and each was measured to determine statistical variance in their performance. The test setup for the measurements is shown in Figure 8-2.

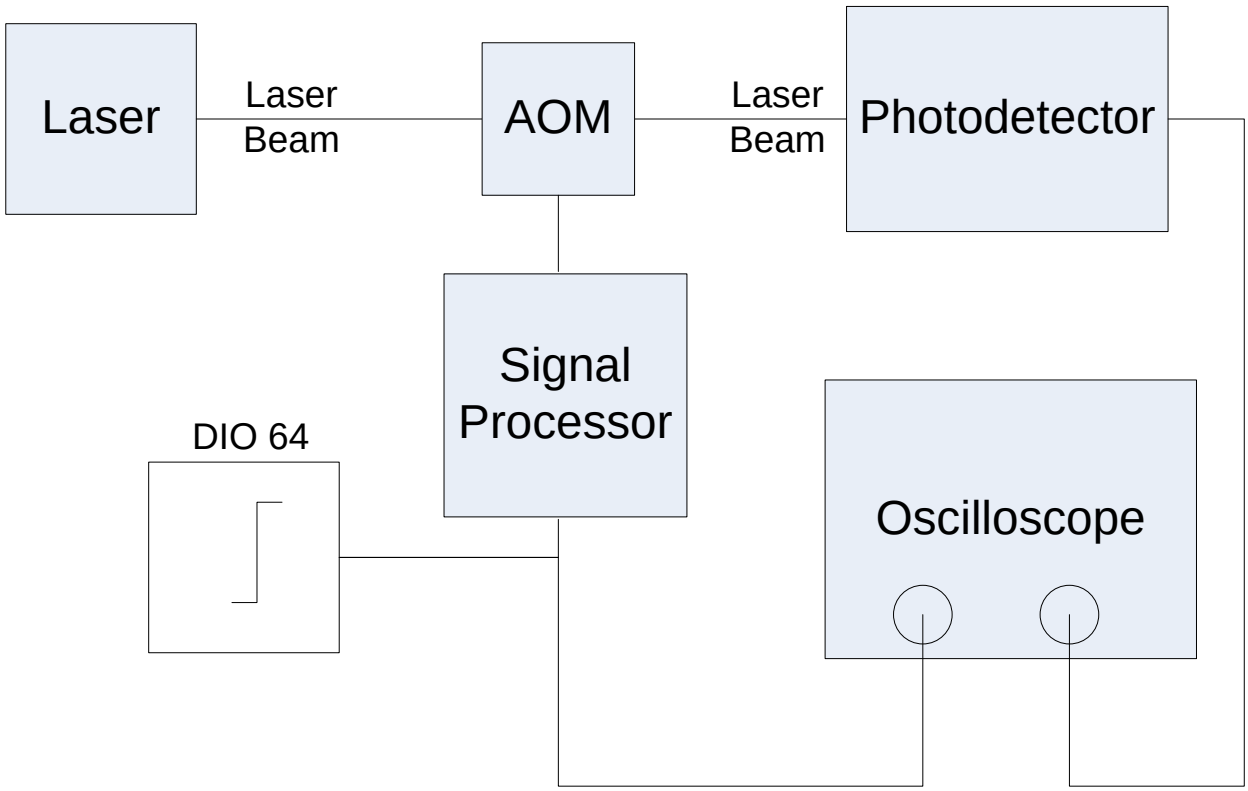

Figure 8-2 - AOM test setup diagram.

The DIO 64 provides a trigger signal to the signal processor that drives the AOM, as well as to the oscilloscope. The laser beam is then diffracted through the AOM and the photo-detector continues to detect the optical power of the 0^{th} order diffracted beam. The output of the photo-detector is sent to the oscilloscope as well. In this way, the oscilloscope can reliably measure the delay between the trigger and the AOM response. Figure 8-3 displays a typical measurement curve of AOM 1 as the light is diffracted.

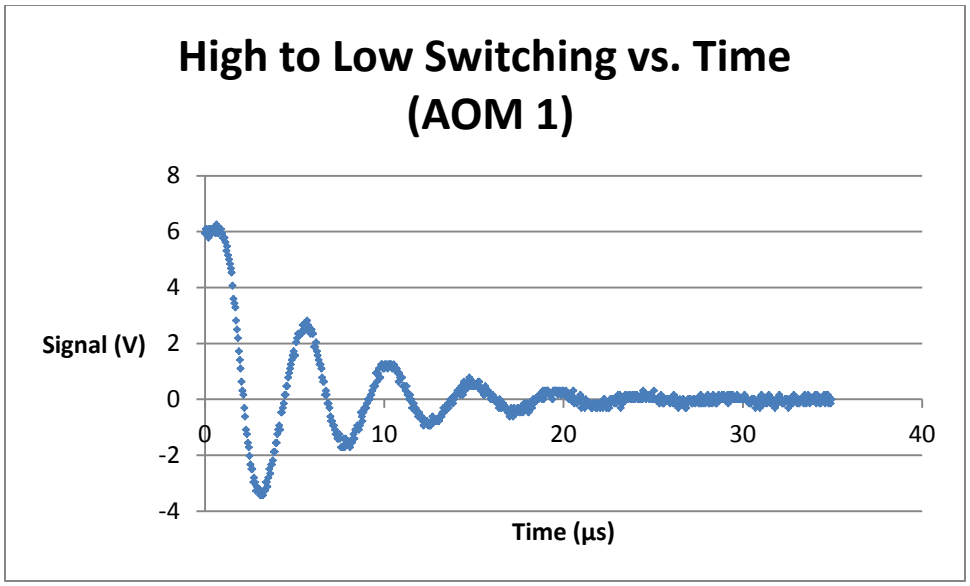

Figure 8-3 - Typical switching curve of AOM.

10 switching curves were measured for all 3 AOMs in the lab and the switching times were recorded for each one. The switching time is defined as the time required for the beam intensity to change from 90 % of its total switching range to 10 % of its total switching range. The switching time T_{switch} is defined in equation (8-1) with V_i being the initial signal voltage, V_f being the final signal voltage, and V_s being the signal voltage.

$$T_{switch} = T|_{V_s=\mathrm{Vi}+0.9(\mathrm{V_f}-\mathrm{V_i})} - T|_{\mathrm{V_s}=\mathrm{Vi}+0.1(\mathrm{V_f}-\mathrm{V_i})} \tag{8-1}$$

The time delay ($\mathrm{T_{delay}}$) between the trigger signal and the beginning of the switching action is defined as the time at which the signal first reaches 10 % of its switching range and is defined in equation (8-2). The measurement of the switching time was done using the MATLAB script in Appendix F.

$$\mathrm{T_{delay}} = T|_{\mathrm{V_s}=\mathrm{Vi}+0.1(\mathrm{V_f}-\mathrm{V_i})} \tag{8-2}$$

Table 8-2 displays the summarized AOM switching data.

Table 8-2 - Summarized AOM switching data

	Low to High Switching		High to Low Switching	
AOM	Start Delay (µs)	Switching Time (µs)	Start Delay (µs)	Switching Time (µs)
1	1.14 ± 0.08	15 ± 3.0	1.18 ± 0.08	14.9 ± 0.9
2	1.23 ± 0.05	11 ± 0.7	1.28 ± 0.05	16.9 ± 2.0
3	1.00 ± 0.04	15.1 ± 1.0	1.06 ± 0.04	14.9 ± 1.0

The data shown in Table 8-2 is sufficient to perform experience using the AOMs. Table 8-3, Table 8-4, and Table 8-5 display the statistical timing data for each measurement of each AOM.

Table 8-3 - AOM 1 statistical switching data

AOM	1	Low To High		
T_{delay} (µs)	T_{end} (µs)	T_{switch} (µs)	Average Start Delay (µs)	1.14
1.25	18.9	17.6	Start Delay Variance (µs^2)	0.00603
1.25	14.0	12.7	Start Delay Standard Deviation (µs)	0.0776
1.10	14.2	13.1	Average Switching Time (µs)	14.7
1.05	25.1	24.0	Switching Time Variance (µs^2)	11.8
1.15	14.0	12.9	Switching Time Standard Deviation (µs)	3.44
1.10	15.9	14.8		
1.20	14.5	13.3		
1.00	14.1	13.1		
1.10	13.6	12.5		
1.15	14.1	13.0		
AOM	1	High to Low		
T_{end} (µs)	T_{delay} (µs)	T_{switch} (µs)	Average Start Delay (µs)	1.18
17.2	1.25	16.0	Start Delay Variance (µs^2)	0.00610
16.9	1.15	15.8	Start Delay Standard Deviation (µs)	0.0781
15.3	1.25	14.1	Average Switching Time (µs)	14.9
17.3	1.10	16.2	Switching Time Variance (µs^2)	0.826
15.2	1.20	14.0	Switching Time Standard Deviation (µs)	0.909
15.7	1.25	14.4		
15.6	1.10	14.5		
17.2	1.05	16.2		
15.3	1.15	14.1		
15.4	1.30	14.1		

Table 8-4 - AOM 2 statistical switching data

AOM	2	Low To High		
T_{delay} (µs)	T_{end} (µs)	T_{switch} (µs)	Average Start Delay (µs)	1.23
1.25	12.2	10.9	Start Delay Variance (μs^2)	0.00213
1.25	12.3	11.1	Start Delay Standard Deviation (µs)	0.0461
1.20	11.9	10.7	Average Switching Time (µs)	11.1
1.25	14.2	13.0	Switching Time Variance (μs^2)	0.465
1.25	12.4	11.2	Switching Time Standard Deviation (µs)	0.682
1.15	11.9	10.7		
1.15	12.5	11.4		
1.25	11.6	10.3		
1.30	12.4	11.1		
1.20	11.9	10.7		
AOM	2	High to Low		
T_{end} (µs)	T_{delay} (µs)	T_{switch} (µs)	Average Start Delay (µs)	1.28
17.7	1.25	16.4	Start Delay Variance (μs^2)	0.00210
23.1	1.25	21.9	Start Delay Standard Deviation (µs)	0.0458
15.9	1.30	14.6	Average Switching Time (µs)	16.9
20.2	1.25	19.0	Switching Time Variance (μs^2)	4.11
15.7	1.30	14.4	Switching Time Standard Deviation (µs)	2.03
18.1	1.20	16.9		
17.9	1.30	16.6		
18.1	1.35	16.8		
17.8	1.25	16.6		
17.9	1.35	16.6		

Table 8-5 - AOM 3 statistical switching data

AOM	3	Low To High		
T_{delay} (µs)	T_{end} (µs)	T_{switch} (µs)	Average Start Delay (µs)	0.995
0.96	15.2	14.3	Start Delay Variance (μs^2)	0.00152
0.96	15.7	14.7	Start Delay Standard Deviation (µs)	0.0391
1.01	17.3	16.3	Average Switching Time (µs)	15.1
1.06	15.7	14.7	Switching Time Variance (μs^2)	0.952
1.01	17.9	16.9	Switching Time Standard Deviation (µs)	0.976
1.01	15.4	14.4		
1.06	15.2	14.2		
0.96	15.9	15.0		
0.96	17.5	16.6		
0.96	15.4	14.5		
AOM	3	High to Low		
T_{end} (µs)	T_{delay} (µs)	T_{switch} (µs)	Average Start Delay (µs)	1.06
15.4	1.00	14.4	Start Delay Variance (μs^2)	0.00123
15.2	1.10	14.1	Start Delay Standard Deviation (µs)	0.0350
17.3	1.10	16.2	Average Switching Time (µs)	14.9
17.5	1.10	16.4	Switching Time Variance (μs^2)	0.944
17.6	1.05	16.5	Switching Time Standard Deviation (µs)	0.972
15.2	1.05	14.2		
15.3	1.05	14.3		
15.4	1.00	14.4		
15.2	1.05	14.2		
15.3	1.05	14.2		

C. Mechanical Shutters

The mechanical shutters provide a necessary component of the MOT/dipole trap laser amplitude switching. The shutters used in the lab are Thorlabs SH05 shutters. They work by employing a electromagnetic solenoid that allows for fast mechanical control of the shutter opening.

C.1 Test Setup

There are three shutters in the lab and each was tested 10 times to discern the average switching time and variance within that switching time. The test setup is shown in Figure 8-4.

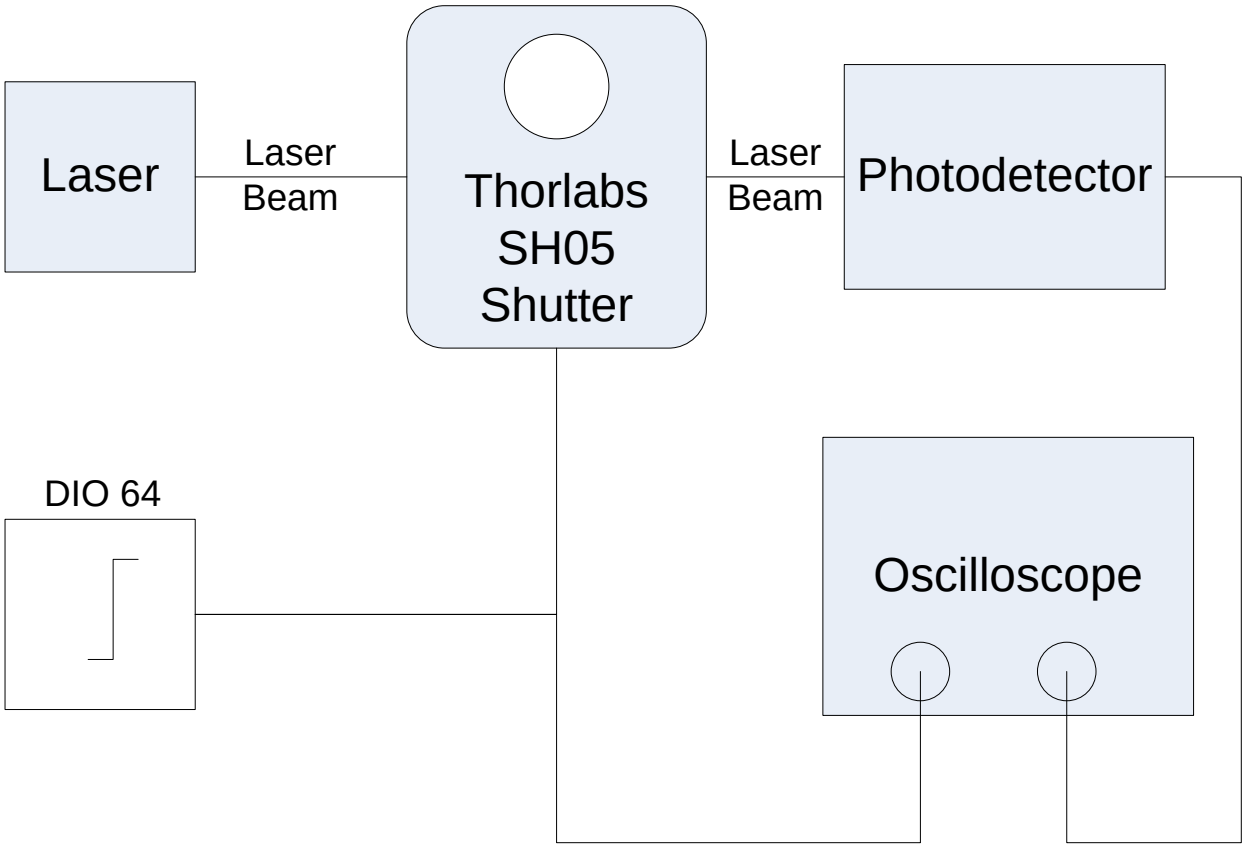

Figure 8-4 - Thorlabs SH05 Shutter test setup.

The DIO 64 sends a trigger signal to the Thorlabs SH05 shutter as well as the oscilloscope for triggering. The measured beam intensity is measured by the photo-detector and sent to the oscilloscope as well. In this way the beam intensity can be indirectly triggered relative to the DIO 64 signal. Switching time is defined using the same criterion as for the AOM switching characterization in Appendix B. Figure 8-5 displays a typical measured switching signal for shutter 1.

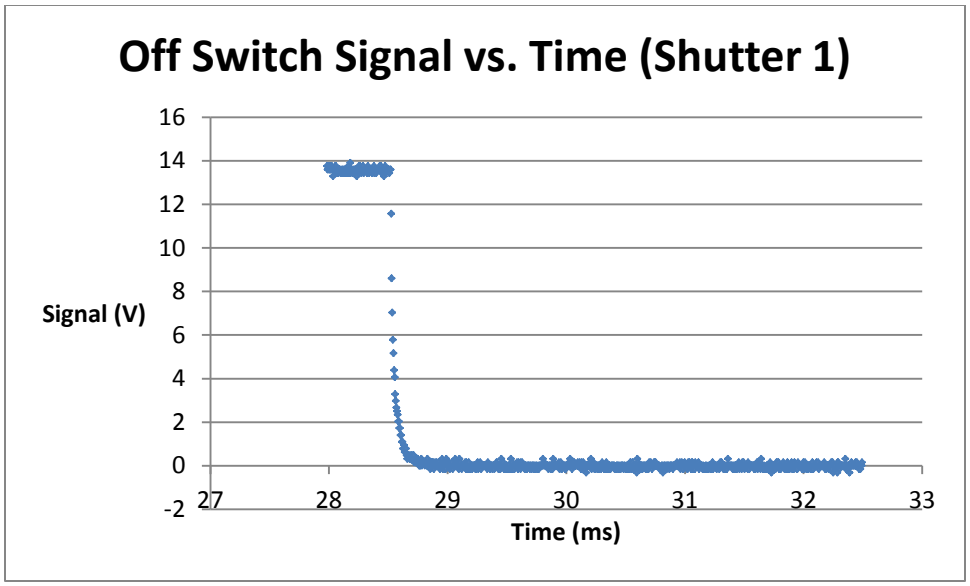

Figure 8-5 - Typical test switching curve for Shutter 1.

10 curves for each shutter in the lab for both on-off switching (High to Low) and off-on switching (Low to High) were measured using the MATLAB script in Appendix F. The summarized statistical switching data is displayed in Table 8-6.

Table 8-6 - Summarized Shutter switching data

	Low to High Switching		High to Low Switching	
Shutter	Start Delay (ms)	Switching Time (ms)	Start Delay (ms)	Switching Time (ms)
1	9.1 ± 0.1	0.8 ± 0.05	28.0 ± 0.5	1.36 ± 0.7
2	7.3 ± 0.1	1.7 ± 0.05	28.2 ± 0.6	1.16 ± 0.5
3	10.0 ± 0.1	1.40 ± 0.05	30.5 ± 1.0	2.15 ± 1.0

The average switching delays for shutters 1, 2, and 3 are similar in number and the standard deviation for any switching characteristic among them is less than 1 ms which makes these switches reliable for the requirements necessary of the MOT to dipole trap transfer process. The tabulated and statistical data for each shutter is displayed in Table 8-7, Table 8-8, and Table 8-9.

Table 8-7 - Shutter 1 statistical switching data

Shutter	1	Low To High		
T_{delay} (µs)	T_{end} (µs)	T_{switch} (µs)	Average Start Delay (ms)	9.05
9.20	10.0	0.80	Start Delay Variance (ms^2)	0.00850
9.10	9.90	0.80	Start Delay Standard Deviation (ms)	0.0922
8.90	9.70	0.80	Average Switching Time (ms)	0.760
9.00	9.70	0.70	Switching Time Variance (ms^2)	0.00240
9.10	9.80	0.70	Switching Time Standard Deviation (ms)	0.0490
9.00	9.80	0.80		
9.00	9.70	0.70		
9.00	9.80	0.80		
9.00	9.80	0.80		
9.20	9.90	0.70		
Shutter	1	High to Low		
T_{end} (µs)	T_{delay} (µs)	T_{switch} (µs)	Average Start Delay (ms)	28.0
28.6	27.6	1.00	Start Delay Variance (ms^2)	0.268
29.6	27.6	2.00	Start Delay Standard Deviation (ms)	0.518
29.3	27.9	1.40	Average Switching Time (ms)	1.36
29.4	29.3	0.100	Switching Time Variance (ms^2)	0.516
28.6	28.5	0.100	Switching Time Standard Deviation (ms)	0.719
29.5	27.6	1.90		
29.5	27.6	1.90		
29.5	28.3	1.20		
30.1	28.0	2.10		
29.8	27.9	1.90		

Table 8-8 - Shutter 2 statistical switching data

Shutter	2	Low To High		
T_{delay} (µs)	T_{end} (µs)	T_{switch} (µs)	Average Start Delay (ms)	7.29
7.30	9.10	1.80	Start Delay Variance (ms^2)	0.00490
7.30	9.00	1.70	Start Delay Standard Deviation (ms)	0.0700
7.30	9.00	1.70	Average Switching Time (ms)	1.73
7.30	9.10	1.80	Switching Time Variance (ms^2)	0.00210
7.30	9.00	1.70	Switching Time Standard Deviation (ms)	0.0458
7.20	8.90	1.70		
7.20	9.00	1.80		
7.20	8.90	1.70		
7.40	9.10	1.70		
7.40	9.10	1.70		
Shutter	2	High to Low		
T_{end} (µs)	T_{delay} (µs)	T_{switch} (µs)	Average Start Delay (ms)	28.2
29.7	28.2	1.50	Start Delay Variance (ms^2)	0.366
29.6	29.4	0.20	Start Delay Standard Deviation (ms)	0.605
29.1	28.2	0.90	Average Switching Time (ms)	1.16
29.3	28.3	1.00	Switching Time Variance (ms^2)	0.298
29.2	27.6	1.60	Switching Time Standard Deviation (ms)	0.546
29.2	27.9	1.30		
29.2	27.6	1.60		
29.3	29.1	0.200		
29.4	27.6	1.80		
29.2	27.7	1.50		

Table 8-9 - Shutter 3 statistical switching data

Shutter	3	Low To High		
T_{delay} (µs)	T_{end} (µs)	T_{switch} (µs)	Average Start Delay (ms)	9.94
9.90	11.3	1.40	Start Delay Variance (ms^2)	0.00640
9.80	11.3	1.50	Start Delay Standard Deviation (ms)	0.0800
9.90	11.3	1.40	Average Switching Time (ms)	1.40
10.0	11.4	1.40	Switching Time Variance (ms^2)	0.002
9.90	11.3	1.40	Switching Time Standard Deviation (ms)	0.0447
10.0	11.4	1.40		
10.0	11.4	1.40		
9.90	11.3	1.40		
9.90	11.3	1.40		
10.1	11.4	1.30		
Shutter	3	High to Low		
T_{end} (µs)	T_{delay} (µs)	T_{switch} (µs)	Average Start Delay (ms)	30.5
32.5	29.7	2.80	Start Delay Variance (ms^2)	0.970
32.7	29.8	2.90	Start Delay Standard Deviation (ms)	0.985
32.6	32.2	0.400	Average Switching Time (ms)	2.15
32.6	30.1	2.50	Switching Time Variance (ms^2)	0.979
32.7	30.1	2.60	Switching Time Standard Deviation (ms)	0.989
32.6	30.1	2.50		
32.6	29.6	3.00		
32.6	29.6	3.00		
32.6	32.3	0.300		
32.6	31.1	1.50		

D. AOM Modulation Switch

Table 8-10 shows a list of the parts used to assemble the AOM modulation circuit. The majority of the functionality of the circuit comes from the ADG918 and the rest of the components serve to bias the circuit properly.

Table 8-10 - AOM modulation switch parts list

Part Number	Part Description	Quantity	Purpose	Unit Price
ADG918	RF switch integrated circuit	1	To control the output of the sine wave generator so that modulation can be activated and deactivated while maintaining AOM beam diffraction.	$2.90
SMA Female Edgemount Connector	SMA connectors that are soldered to the edge of a PCB	2	To connect BNC cables to the analog switch circuit.	$0.50
4350 Duroid PCB	30 mil thick 4350 Duroid substrate 1/2 oz copper board	1	To mill circuit traces to feed the ADG918 switch	$0.00
1N4007	Diode	1	To bring the bias level of a 2 AA battery case down to acceptable levels for the ADG918.	$0.11
Magnetic Wire	26 gauge Magnetic Wire	1	To connect the ADG918 leads to the milled PCB.	$0.00
4 kΩ resistor	Resistor	1	To be part of a voltage divider to translate the digital control signal to a level compatible with the ADG918 digital logic levels.	$0.10
5 kΩ resistor	Resistor	1	To be part of a voltage divider to translate the digital control signal to a level compatible with the ADG918 digital logic levels.	$0.10
50 Ω resistor	Resistor	1	To terminate the AOM signal generator while the switch is turned off.	$0.10
Total Price				$4.31

Figure 8-6 displays the AOM modulation switch's circuit diagram composed of the parts listed in Table 8-10.

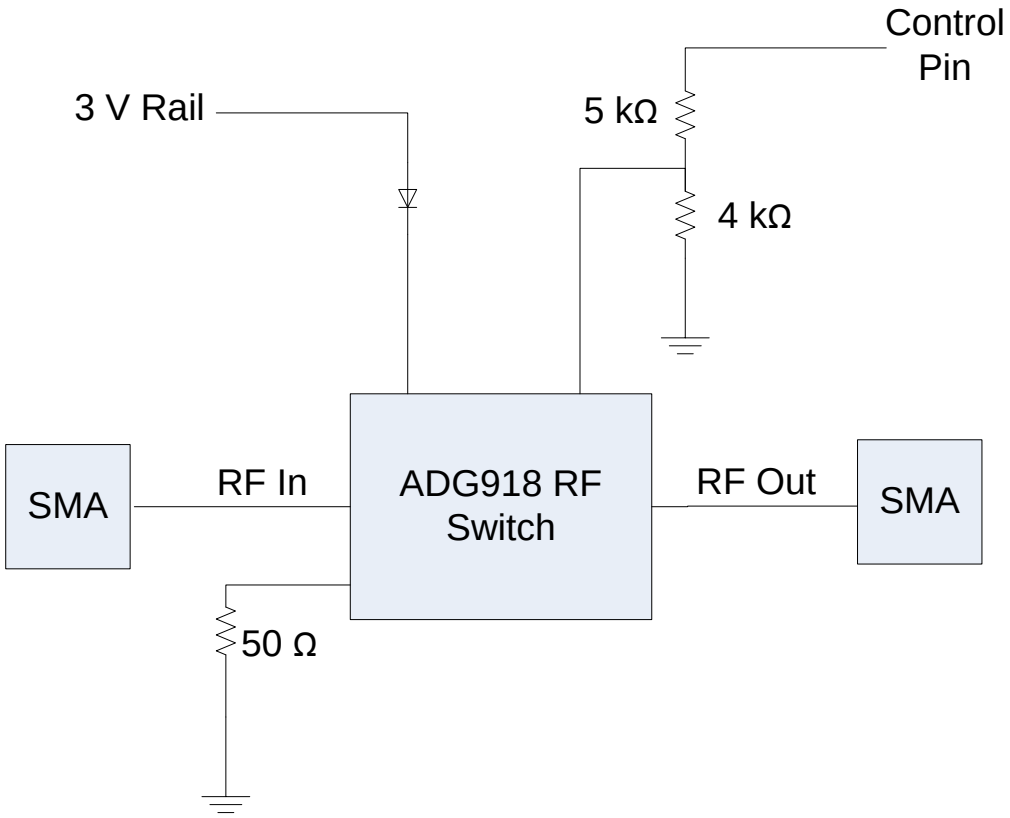

Figure 8-6 - AOM modulation switch circuit diagram.

The layout for the AOM board that was milled to generate properly wide traces is shown in Figure 8-7. The ADG918 was soldered to the board using magnetic wiring.

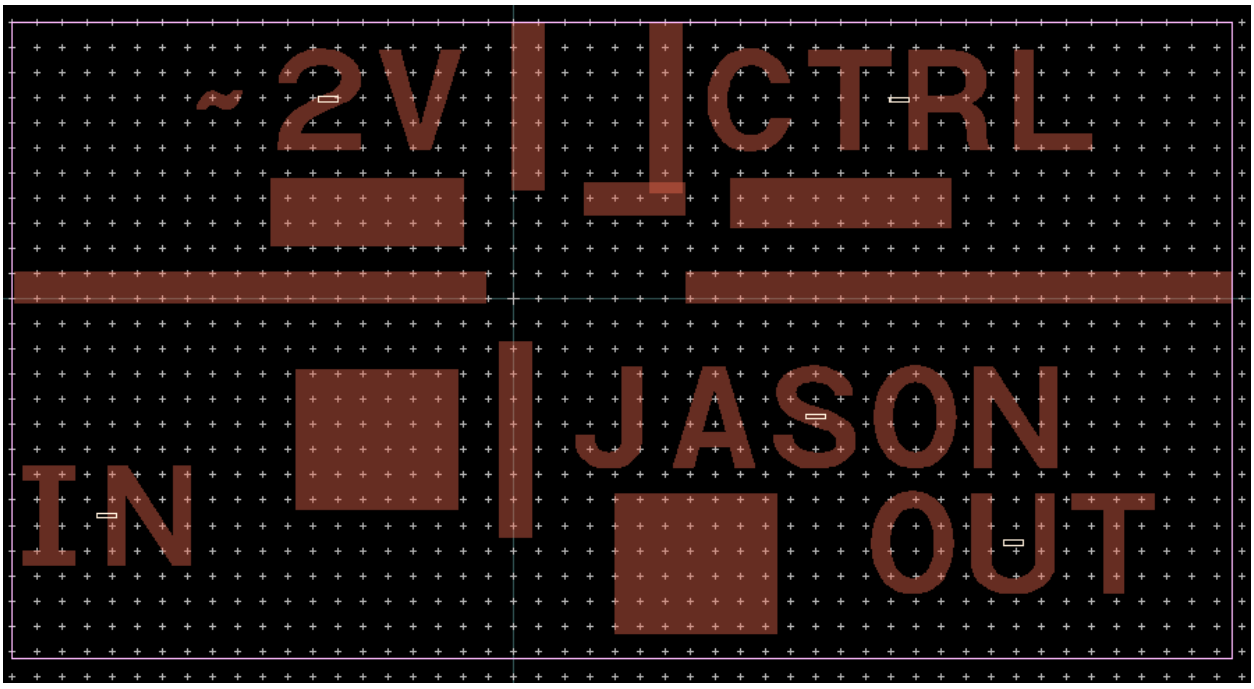

Figure 8-7 - AOM modulation switch board layout.

E. DIO 64

The DIO 64 is a computer input/output board created by Viewpoint Systems to send and receive digital signals at high frequencies. The board can be controlled by C and by LabVIEW. For this project, LabVIEW was chosen due to the pre-existing control modules that came with the DIO 64 board and due to the fact that many other systems in the lab are also controlled by LabVIEW making the future system integration possible.

E.1 User Interface

For lab use, "Output Data.vi" is sufficient. Below in Figure 8-8 is the user interface for this LabVIEW program.

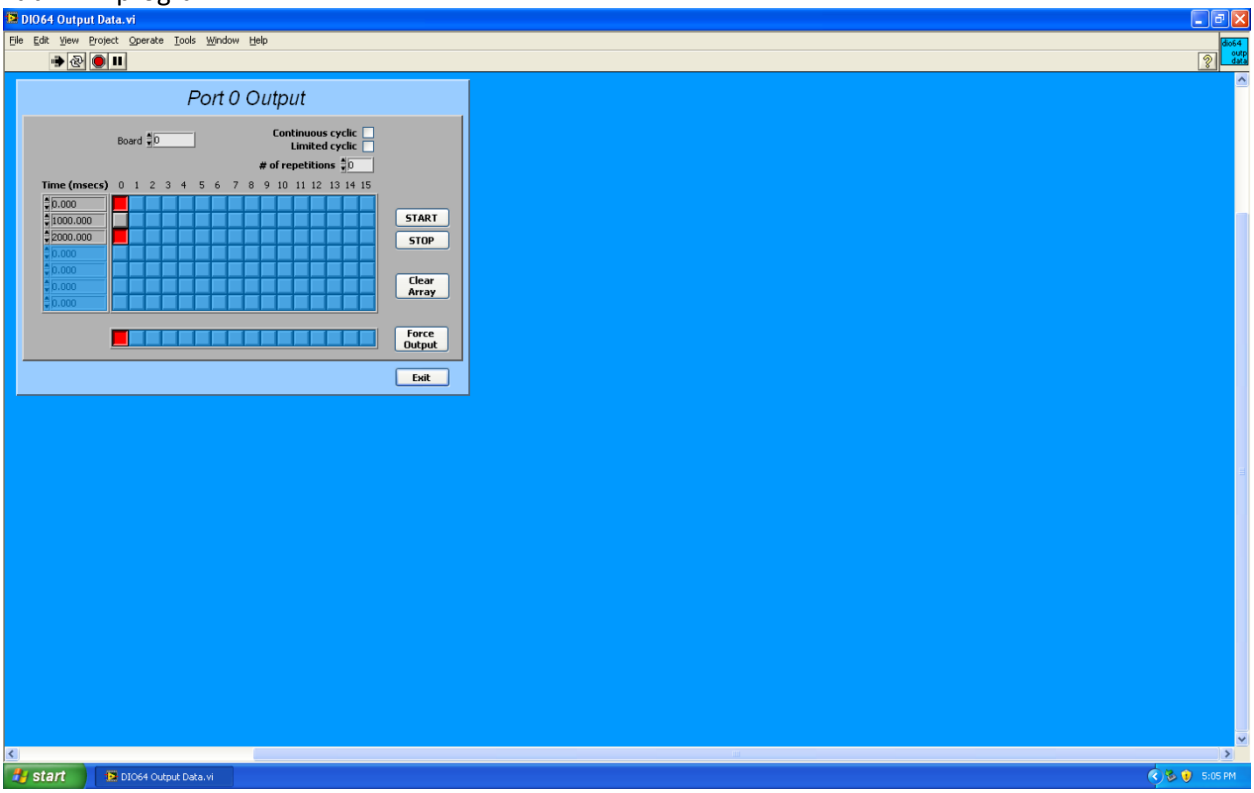

Figure 8-8 - DIO 64 user interface.

The general program flow goes as follows: Run LabVIEW, press the START button, press the STOP button, and then select your desired output value/time pairs. Every time that you press the START button the DIO 64 will produce the programmed output waveforms (Be sure to always press STOP after the waveform has finished executing). The FORCE OUTPUT button can be used to set the initial DIO 64 output values as well.

F. Switching Characteristic Analysis MATLAB Script

The following MATLAB script was used to analyze recorded switching data in .csv format from oscilloscope measurements. The trigger signal is fed through probe 2 and the measured waveform is fed through probe 1 on the oscilloscope for this script.

```
function [ Th, Tl ] = HighLow( file )
%function [ Th, Tl ] = HighLow( file )

percent = 0.1;
A = xlsread(file);
t = A(2:end,1);
s = A(2:end,2);
if(s(1) > s(end))
    maximum = s(1);
    minimum = s(end);
else
    maximum = s(end);
    minimum = s(1);
end
delta = maximum-minimum;
high1 = maximum - percent*delta;
high2 = maximum + percent*delta;
low1 = minimum + percent*delta;
low2 = minimum - percent*delta;
search = find(diff(sign(s-high1)));
h1 = search(end);
search = find(diff(sign(s-high2)));
if(isempty(search))
    h2= h1;
else
    h2 = search(end);
end
search = find(diff(sign(s-low1)));
l1 = search(end);
search = find(diff(sign(s-low2)));
if(isempty(search))
    l2 = l1;
else
    l2 = search(end);
end
Th = t(max(h1,h2));
Tl = t(max(l1,l2));
end
```